CHALMERS
UNIVERSITY OF TECHNOLOGY

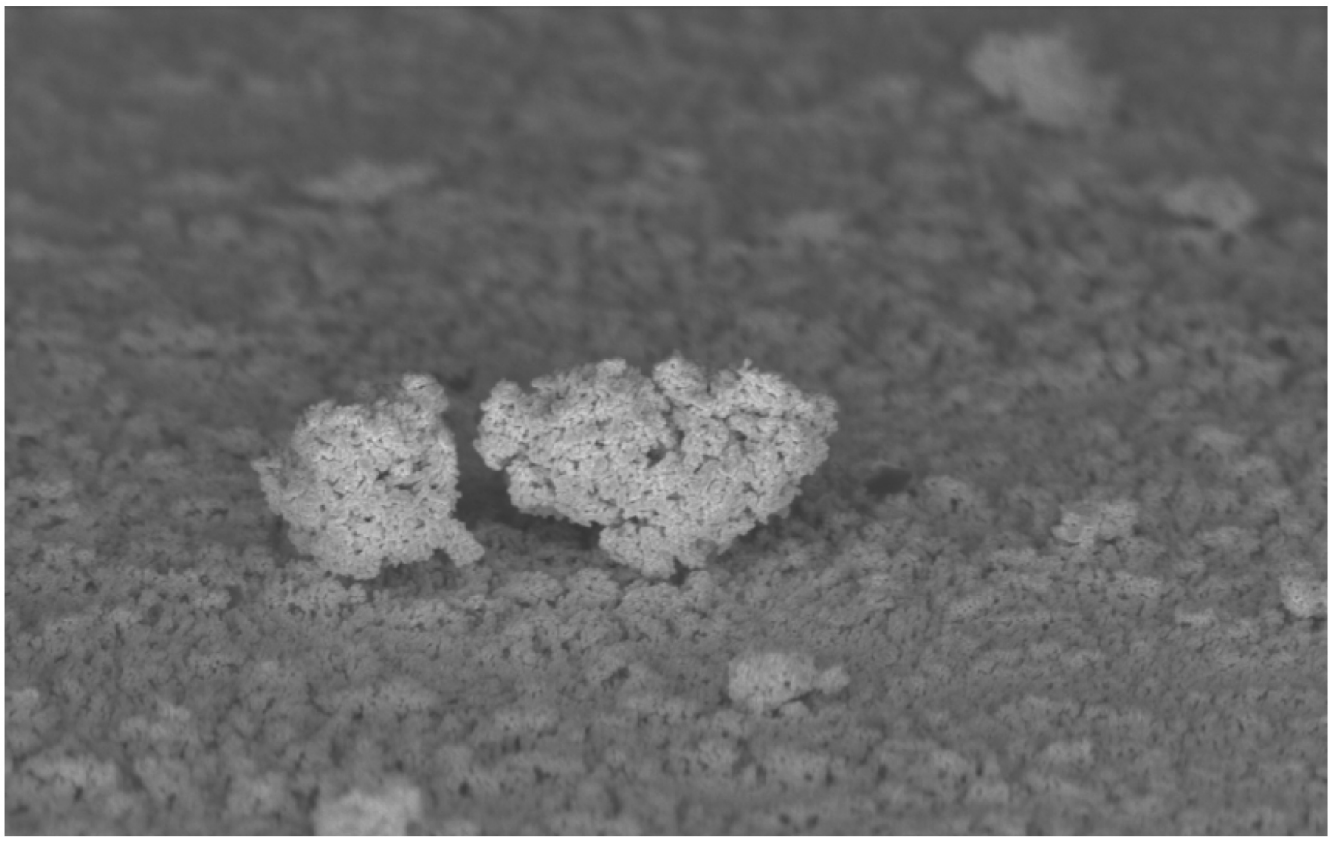

# Production of green fuels via electrochemical reduction of $CO_2$ on nanoporous gold electrodes

## Roughness factor dependence of the catalytic activity

Master's Thesis in Sustainable Energy Systems

Pascal Gebauer

Department of Applied Physics / Division of Chemical Physics
CHALMERS UNIVERSITY OF TECHNOLOGY
Gothenburg, Sweden 2014

# Production of green fuels via electrochemical reduction of $CO_2$ on nanoporous gold electrode

Roughness factor dependence of the catalytic activity

*Master's Thesis within the Sustainable Energy Systems programme*


Pascal Gebauer

Department of Applied Physics
Division of Chemical Physics
Chalmers University of Technology
Gothenburg, Sweden 2014

Production of green fuels via electrochemical reduction of $CO_2$ on nanoporous gold electrode


Master's Thesis report within the Sustainable Energy Systems programme
Department of Applied Physics
Division of Chemical Physics
Chalmers University of Technology
SE-412 96 Gothenburg // Sweden 2014
Telephone: + 46 (0)31-772 1000

SUPERVISOR:
Björn Wickman, Chalmers University of Technology

EXAMINER
Assistant Professor Christoph Langhammer, Chalmers University of Technology

**Abstract**

Electrochemical reduction of $CO_2$ is a research direction within electrochemistry that adresses environmental probems related to $CO_2 emissions$.$CO_2$ is reduced in the presence of a catalyst material and an electrolyte to hydrocarbons by providing energy to the process. The technique promises a pathway towards a carbon neutral energy cycle by using renewable as an energy source. In this Master's thesis a set-up for electrochemical reduction of $CO_2$ has been assembled, calibrated and its successful operation verified by repetition of literature results on a Cu electrode. Additionally, Au electrodes with different roughness factors have been produced in order to analyse the influence of the surface structure on the selectivity of the reduction of $CO_2$ to $CO$ and the decrease of overpotential for this reaction as reported in literature before. The reduction products of $CO_2$ electrolysis are dependent on the electrode material, topography and other electrochemical parameters like pH, mass transport, pressure and temperature. The gas products are measured in a closed system with a gas chromatograph. In this work copper and gold electrodes were used with a limitation of gaseous products that are mainly hydrogen, carbon monoxide, methane, ethane, ethylene and propylene for copper and only carbon monoxide for gold. Gold was chosen as electrode due to its low overpotential to form CO that is used as a bulk chemical for methanol production and the Fischer–Tropsch process. Verification of the set-up has been done by comparing results from literature on a plane copper electrode in aqueous 0,1 M $KHCO_3$ solution with the performance in this set-up. The results differ from Hori's results what was traced back to contaminations on the copper electrode and changed conditions at the electrode surface. A carbon coverage of the copper surface was observed after electrolysis. Au electrodes were produced by beam evaporation of a 100 nm Au film on a silicon substrate. Nanoporous gold (NPG) electrodes have been used to estimate the dependence of the surface roughness and structure on the selectivity of gold towards $CO$ synthesis. The NPG films were produced with an electroplating technique based on the reduction of gold oxide in the anodic potential region and deposition of dissolved Au in the cathodic region. The method to control the roughness was based on slow cathodic sweeps to different low potentials and the number of sweeps. 5 different gold electrodes (RF2, RF6, RF10, RF15, RF17) with different roughness factors (RF) have been produced and the evaporated gold film was measured to have a roughness factor of 1.05. The RF was measured with underpotential deposition of copper ions and with analysis of the gold-oxide reduction peak in acidic solution. The results for these electrodes were contradictory. Whereas it was possible to measure a reduction series for RF1 and RF10 without obvious problems between 0.25 V and 0.6 V vs. RHE, other electrodes showed signs of contaminations. The selectivity towards $CO$ for RF6 dropped after 40 min electrolysis and remained on a low level. Anodic polarization was used to remove contaminants on the surface after each potential step and electropolishing was conducted prior to the experiments. Whereas this method seemed to be successful for RF10, RF15 showed a very low selectivity for $CO$. In order to analyse the type of contamination XPS measurements of the electrodes were conducted. The results showed a contamination with copper and carbon on the gold electrodes. Copper ions could have remained in the cell after electrolysis with $Cu$ electrodes or they could come from a copper foil which is used to mount the Au samples on a metal conductor. Carbon contamination was already observed on the copper electrode but the Au sample were also exposed to air before XPS measurements. The topography of the electrodes was analysed with a scanning electron microscope (SEM). The images showed an increasing film thickness for rougher electrodes from several 100 nm to about 2$\mu$m for RF17. Whereas the evaporated samples are very flat with a packed and even structure, the rougher electrodes show distinctive clusters and particles. The particle size does not alter with RF and the oval shape is about 200 nm in length and 150 nm in width whereas the cluster size increases with roughness. This

suggests that the dimension of the nano particles might be the dominant factor rather than the roughness factor.

## Preface

This thesis work, starting in January 2014, has been performed at Chalmers University of Technology within the department of Applied Physics and in the division of Chemical Physics. I would like to thank my supervisor Björn Wickman for guidance and support with many questions. He gave me the opportunity to learn a lot during discussions and was always available when problems occured. Also I would like to thank him for fabricating many Au samples in many sessions in the clean room. I would like to thank my supervisor Christoph Langhammer. I would also like to thank Beniamino Landolo for his support with ohmic drop compensation of the set-up and for the permission to use some of his chemicals. Additionally I want to mention Lars Hellberg and thank him for his support with the XPS system as well as Ferry Nugroho for his support with SEM. Finally I would like to thank everyone at Chemical Physics for providing a friendly atmosphere.

Gothenburg, Sweden September 2014

Pascal Gebauer

# Contents

# List of Figures

## List of Abbreviations

| | |
|---|---|
| CE | Counter electrode |
| CV | Cyclic voltammogram |
| FID | Flame ionization detector |
| FID Back | Back detector of the Gas Chromatograph detecting $CH_4$ after conversion form CO by a Nickel catalyst |
| FID Front | Front detector of the Gas Chromatograph detecting hydrocarbons |
| GC | Gas chromatograph |
| NPG | Nanoporous gold |
| OER | Oxygen evolution reaction |
| RE | Reference electrode |
| RF | Roughness factor |
| RHE | Reversible hydrogen electrode |
| SEM | Scanning electron microscope |
| TCD | Thermal Conductivity detector |
| UPD | Underpotential deposition |
| WE | Working electrode |
| XPS | X-ray Photoelectron Spectroscopy |

# 1

# Introduction

It is well known and accepted that $CO_2$ as an exhaust gas from fossil fuel fired power plants or vehicle engines has a huge influence on climate change and can be considered as a greenhouse gas. Hence, efforts to mitigate the impact of $CO_2$ on the global climate mainly focus on the prevention of $CO_2$ emissions. By using renewable energy sources instead of $CO_2$ forming fuels, abatement of emissions might be an alternative pathway. But this approach will require significant changes within the energy system. A different approach is the recycling of $CO_2$ by electrochemical reduction to form hydrocarbons or useful chemicals like methane, methanol, ethanol, urea or formate. Such reactions could be considered as $CO_2$-neutral since the required energy could come from intermittent renewable energy sources during off-peak hours. In addition, fuels made from reduced $CO_2$ serve as an gaseous or liquid storage of chemical energy, what could be used in the transportation sector or chemical industry. The choice and morphology of catalysis material are the key factors which decide about the selectivity of synthesis towards certain compounds. Hori at al. [1] showed already in 1986 that direct reduction of $CO_2$ with reasonable current densities and rather high faradaic efficiencies is possible on a copper foil electrode but in the expense of a rather high overpotential. In summary, electrochemical reduction of $CO_2$ can reduce the $CO_2$ emissions to the environment from many industrial applications, produce $CO_2$ neutral fuels and store electricity as chemical energy. Hence, this process has seen a large increase of interest in the last years but is still not understood completely. The focus in current research is on the selection of appropriate electrode elements and morphology that provide a high selectivity at low overpotentials. The goal of this work is to make a contribution to this research by analyzing different surface structures of NPG films deposited on a semiconductor material as a catalyst subsequent to the project of Kanan in 2012 [2]. In this work a set up for electrochemical reduction of $CO_2$ is tested, improved and verified by means of comparing results of a plane copper electrode with the results of for example Hori. [3] Electrochemical reduction is conducted in electrochemistry which is a part of physical chemistry. Electrochemistry focusses on electrode processes, e.g. charge transfer on the interface of an solid (electrodes) and a liquid (electrolyte) phase. Several techniques, i.e. cyclic voltammetry, chronopotentiometry and chronovoltammetry, were applied in this work. All have in common that very small changes of voltage and current in an electrochemical system can be measured. This is important since the reduction of $CO_2$ takes place on the surface of an electrode in the sense that each molecule participating in the electrode process is important. Reduction products were measured by gas chromatography combined with several detectors. The electrode surfaces were studied with surface sensitive measurement techniques, Scanning electron microscope (SEM) and XPS. Reduction of $CO_2$ is done in 0,1M potassium hydroxide ($KHCO_3$) by voltammetric and chronopotentiometric measurements in a three compartment cell. The second part of this work focusses on the question whether an increase of the Roughness

factor (RF) of a gold electrode improves the overall performance of the electrode in terms of lower overpotentials and higher faradaic efficiencies for hydrocarbons. Thereforem gold was evaporated on silicon wafers by thin-film deposition in order to obtain a rather plane surface. From this initial step additional gold particles were electrodeposited with the aim of increasing the roughness factor by several orders and fabricate a NPG film.

# 2

# Background and Theory

In this chapter the basic principles of electrochemistry are explained. Further on background information of electrochemical reduction of $CO_2$ is provided including important developments, parameters and techniques used in this thesis.

## 2.1 Electrochemistry

### 2.1.1 Fundamentals

Electrochemistry as a part of physical chemistry focusses on chemical reactions at the interface of a solid, molten and a liquid phase. Chemical reactions include charge transfer at the boundary of an electrode (conducting or semiconducting phase) and an electrolyte or a species in solution (ionically conducting phase). The reactions taking place at the electrode are dependent on the concentration of an electroactive species which are in molecular distance to the electrode surface, thus transport processes close to the solid/liquid boundary are of interest. A typical electrode reaction in an electrochemical cell consists of an oxidation process, a reduction process and an electron transfer. At the anode the oxidation occurs, which means that there is a charge transfer from the electrolyte to the electrode. The electron is transferred from the anode to the cathode and reacts with an electroactive species on the surface of the cathode. i.e. the electroactive species is reduced by the electron transfer. The product of the reactions can be liquid or gaseous and leave the surface or it can be solid and deposit on the surface. Since the electron is transferred from the anode to the cathode both reactions are interconnected. The reactions at both electrodes are in fact electrochemical half-reactions and contribute to the overall cell reaction of the electrochemical cell. The electrolysis of water is an example for such a reaction. Hydrogen evolution occurs at the cathode whereas oxygen evolution takes place at the anode. As electrolyte diluted sulphuric acid can be used in order to increase the conductivity. The half cell reactions and the cell reaction are written below. In order to have a

$$\begin{array}{ll} \text{Cathode} & 4H_3O^+ + 4e^- \longrightarrow 2\mathrm{H}_2 + 4H_2O \\ \text{Anode} & 6H_2O \longrightarrow O_2 + 4H_3O^+ + 4e^- \\ \text{Cell Reaction} & 2H_2O(l) \longrightarrow 2H_2(g) + O_2(g) \end{array}$$

continuous reaction in a cell the species participating in the reactions have to be continuously absorbed on the electrode's surfaces. The mass transport in the electrolyte cell is therefore of importance. On one hand reaction products have to be removed from the surface, on the other hand electroactive species have to be supplied to the surface. Three forms of mass transport

are important for a continuous reaction. Diffusion is the movement of a species due to a concentration gradient. If the species reacts on the surface there is a unequal concentration which leads to a mass transport of reactant to the electrode. However, diffusion is a rather slow process which might lead to mass transport problems. Convection is the movement of molecule due to density or temperature differences within the electrolyte. It arises either from external forces in the electrochemical cell like vibrations, flushing the solution with a gas or a mechanical stirrer. Natural convection in the cell occurs at the electrode surface because density changes due to the reactions. Migration is the movement of charged molecules in the electrolyte due to potential gradients. As already stated, electrons flow from the anode to the cathode. At the cathode there is an agglomeration of negative charge and hence a potential difference compared to the anode. The electrolyte can be charged positive and negative due to dissociation of ionic compounds into ions. A charge difference is called potential and leads to a potential field in the electrolyte which causes electrostatic forces on the molecules. In order for a reaction to happen the reaction must be energetically feasible or thermodynamically favourable. This depends on the energy balance of the reaction. For a chemical reaction that is thermodynamically favourable the Gibbs free energy is negative $\Delta G < 0$. In an electrolyte such a reaction would imply an electron transfer between electrodes and the free energy could be used (Heat, electricity). For a chemical reaction that is thermodynamically unfavourable the Gibbs free Energy is positive ($\Delta G > 0$). The energy difference needs to be supplied in order to start the reaction or shift it towards the desired side of the equilibrium. If there is no change in Gibbs energy ($\Delta G = 0$) the reaction is either not happening or the reaction is in a chemical equilibrium, i.e. the reaction occurs in both direction at the same rate. The Gibbs energy can be expressed in terms of kJ per mol or converted in a cell voltage. The relationship between the Gibbs Energy and the equilibrium cell potential is:

$$\Delta G = -z \cdot F \cdot E^{e}_{cell} \tag{2.1}$$

where -z is the number of transferred electrons in the reaction, F is the *Faraday constant* and E the equilibrium cell voltage. A certain current passing through a conductor faces a certain resistance of the conductor. In order to overcome this resistance a slightly higher potential must be applied to account for the "'losses"' due to the resistance. The same accounts for the electrolyte resistance, the lower the conductivity of the electrolyte, the higher the resistance of the liquid phase. The electrolyte conductance of the solution depends on the cell geometry (area and distance between electrodes) and material dependent properties like ion concentration, type of ions, the viscosity, the temperature and also the electric field of the electrodes that force the ions to move. The sum of the material dependent properties is called conductivity and can be found for different electrolytes in literature [4]

The cell potential $E_cell$ must be supplied in order to start the reaction, however to reach a significant reaction rate for the favourable reaction an overpotential $\eta$ must be applied on both electrodes. In summary a thermodynamically favourable reaction in an electrochemical cell takes place, if the applied cell voltage is higher than the equilibrium cell voltage of the reaction, if it has a significant overpotential and if it accounts for resistive losses in the system:

$$E_{cell,system} = -E^{e}_{cell} - \eta_{cathode} - \eta_{anode} - IR_{solution} - IR_{system} \tag{2.2}$$

If the applied energy is lower than the energy needed to start the reaction or if there is no energy source there is still an interaction between the electrolyte and the electrode. In the half cells the electroactive species are interacting with the electrode. The interaction depends on the chemical potential of the surface atoms on the electrode and on the ions in the electrolyte. Particles tend to go from higher chemical potentials to lower chemical potentials, comparable

to the principle of gravitational potential. If in a half cell a metal electrode is submerged in an electrolyte consisting of its own metal ions, metal ions from the surface will be released into the solution, if the surface has a higher chemical potential. On the other hand, if the electrolyte has a higher potential the ions will deposit on the electrode. This process implies a transfer of charge. If there is no electric circuit there will be an agglomeration of charge at the surface of the electrode, since the positive ions release an electron when depositing on the surface. This agglomeration will lead to a potential difference between the liquid and the solid phase which is called Galvani potential difference. So, if the chemical potential of the electrode is higher, metal ions (positive)$Me^+$ are released at the phase boundary and a so called monolayer of ions is established at the electrode. The positive charge acts as an insulator and inhibits further dissolution of ions. Due to coulomb forces there is a second layer of negatively charged ions attached to the monolayer, a so called electric double layer is established. H. Helmholtz was the first researcher who described a model of the double layer in 1853. [5] He predicted that the double layer formation has the properties of a capacitance and thus it is called double-layer capacitance, whose magnitude is linearly dependent on the voltage applied. But due to Van-der-Waals forces even without current flow a capacitance can be detected, a so called dipole layer is established. The Helmholtz-model was further developed by Gouy-Chapman, Stern, Grahame, Bockris/Devanthan/Müller, Trasatti/Buzzanca, Conway and Marcus. It can be determined by measuring the total charge passed in a voltage region, where no reaction occurs. The Galvani potential difference cannot be measured easily, since the scale is too small. However there is an equilibrium reached in the half cell, when the double layer is set up. Connecting two different half cells to a voltmeter without letting charge pass makes it possible to measure the potential between the equilibriums in the half cells. But since the absolute value of chemical activity in the cells is unknown, the measured voltage difference cannot be analysed, since a closed circuit will change the equilibrium state. It is necessary to compare the half-cell voltages to a reference voltage that does not change over time and is not affected by the cell reaction. A reference system is a half-cell which cell reactions are well known and stable and are chosen to be equal to 0V. In Electrochemistry the Standard Hydrogen Electrode is such a half cell and will be explained later on. Assuming a half cell with an inert electrode whose surface electrons will not dissolve in solution a similar model can be described. An electroactive species in the electrolyte can be oxidized or reduced at the surface of the electrode by releasing or accepting an electron through the electrode. Thus, it is not ions that are exchanged but electrons via the surface area. The equilibrium state is still reached when there is a double layer established. The Galvani potential difference is still dependent on the chemical activity. Although it cannot be measured, it can be calculated form the Nernst Equation. This equation gives the relationship between the concentration or activity of the participating species and the reduction potential of a half cell.

$$E = E^0 + (RT/nF)ln(\alpha_{ox}/\alpha_{red}) \tag{2.3}$$

$E^0$ is the potential of the reference system, R is the universal gas constant, T is the Temperature in the cell in Kelvin, n the number of electrons transferred in the half cell reaction and F the *Faraday constant*. It must be emphasized that the potential is only dependent on the ratio of the activities, not on the actual value. Under standard conditions the Nernst Equation is changed to:

$$E = E^0 + (0{,}059/n)ln(\alpha_{ox}/\alpha_{red}) \tag{2.4}$$

It can be shown that equation (2.4) can be written as:

$$\Delta G = \Delta H - T\Delta S \tag{2.5}$$

with

$$\Delta H = \sum_{R,P} v_P \Delta H_P - v_R \Delta H_R \tag{2.6}$$

$$\Delta S \sum_{R,P} v_P \Delta H_P - v_R \Delta H_R \tag{2.7}$$

where R refers to the reactants and P refers to the products. This makes it possible to obtain $\Delta G$ from standard enthalpies of formation and standard entropies of the reactants and products. As a specific example related to this work the reduction of $CO_2$ to $CO$ is shown.

$$CO_2 + 2H + +2e - - > CO + H2O$$

The standard enthalpy of formation for $CO_2$ is -393.509 $kJ/mol$, for $H^+$ by definition equal to 0, for carbon monoxide it is -110.525 $kJ/mol$ and finally for liquid water -285.8 $kJ/mol$. With (2.6) and (2.7) $\Delta G$ is -18.7071 kJ and the equilibrium voltage is 0.096V.

| Substance | $CO_2$ | $H^+$ | $CO$ | $H_2O$ |
|---|---|---|---|---|
| $\Delta H$ kJ/mol | -393.5 | 0 | -110.5 | -285.25 |
| $\Delta S$ J/mol | 214 | 0 | 198 | 70.12 |

**Table 2.1:** Enthalpies and Entropies of formation at 298 K.

### Electrochemical cells

Electrochemical cells are most widely used with three compartments. The Anode and Cathode compartment, containing the counter respectively working electrode, are separated by an ion-exchanger. Most frequently selective ion-exchange membranes are used in electrochemical cells. Selective means, that they either exchange positively charged cations (cation exchangers) or negatively charged anions (anions exchangers). The third compartment contains the reference electrode. All electrodes are connected to a potentiostat that controls either the voltage or the current across the electrodes.

### Reference electrodes

A two half-cell set up only gives the possibility to measure the potential difference relative to the two cells. But changes of ion activity due to reactions make it impossible to classify this voltage difference. A reference system with a stable ion activity needs to be established. Reference electrodes are divided as electrodes of the first kind and the second kind. The potential of electrodes of the first is directly connected to the ion activity in the solution it is submerged in. All metal electrodes submerged in electrolytes containing their own metals belong to these electrodes.

$$Me^+(aq) + e^- \rightleftharpoons Me_s \tag{2.8}$$

The potential depends on the concentration of metal ions. If the concentration is hold constant then the activity of the ions is constant and an equilibrium state is reached. Other well-known electrodes of the first kind are hydrogen electrodes. Here, platinised platinum sheets are submerged in an acid solution and pure hydrogen gas is flushed through the half cell. The half-cell reaction is the following:

$$H^+(aq) + e^- \longrightarrow H_2$$

The partial pressure of hydrogen gas is 1 bar and hydrogen ions have unit activity. A derivation of the standard SHE hydrogen electrode is the reversible hydrogen electrode RHE. The drawbacks of electrodes of the first kind are the requirement of a well-known ion concentration in the electrolyte, very pure hydrogen gas and a high sensitivity against impurities. Impurities may deposit on the platinum electrode and change the equilibrium state. Reference electrodes of the second kind are not directly dependent on the activity of the surrounding ions. A metal electrode and its own ions are used again, but the number of ions is determined by the electrolyte solubility of a salt containing the same metal ions. In this work a saturated mercury sulphate second kind electrode (MSE) is used. It uses $K_2SO_4$ as internal electrolyte and has a potential of +0.65 V vs. NHE at 25°C.

**Reaction parameters: Current density, faradaic efficiency, overpotential**

In order to estimate the performance of an electrochemical cell to compare different cells several current related parameters can be extracted. The first parameter is the current density. The current density refers to the number of electric current per cross sectional area of the cathode and hence has the unit I/A in mA/cm². Obviously the current density is dependent on the applied voltage and is an indication for reaction process occurring on the electrodes. Each electrode transferred comes from an oxidation process at the anode and is transferred to the cathode. The current density does not give an indication which reaction is happening. If the products of an electrochemical reaction can be measured analytically for example in a mass spectrometer or a gas chromatograph the current density can be used to calculate the current efficiency. In a closed system the number of product molecules in the reduction process is directly dependent on the electric current transferred. If the amount of product molecules or moles is known as well as the total current transferred in a certain timespan, the current efficiency can be calculated by:

$$\epsilon_{k,Faradaic} = \frac{z \cdot n \cdot F}{Q} \tag{2.9}$$

where z is the number of electrons needed for the reduction to a product, n is the number of moles produced, F is Faraday constant and Q the total charge transferred from the anode to the cathode. The third parameter comes from the concept of overpotential. The potential of a half cell against a reference electrode is an indication for the energy balance of a cell and a reaction. Regarding a reaction in an electrochemical cell, the overpotential of this cell is the difference between the standard potential of the reaction and the applied potential in order to start the reaction. Different cell set ups have a different overpotential for the same reaction. The standard potential can be seen as an ideal theoretical case, as stated above. The overpotential can be expressed as an energetic efficiency and is calculated by:

$$\epsilon_{energetic} = \sum_k \frac{E_k^0 \cdot c\epsilon_{k,Faradaic}}{E_k^0 + \eta} \tag{2.10}$$

where $E_k^0$ refers to the equilibrium cell potential of a reaction for a certain product. $\eta$ is the sum of overpotentials on the anode and cathode. $\epsilon_{k,Faradaic}$ is the faradaic efficiency for a product k and will be introduced next. The equation states clearly that low overpotentials and high faradaic efficiencies lead to a high energetic efficiency. In summary, an electrochemical reaction in different set ups can be compared by the faradaic efficiency, current density and the electrode overpotential. From the faradaic efficiency information about the selectivity for a certain electrochemical reaction in a cell can be achieved. The selectivity states the ratio between a desired products from the reactants that have reacted and is therefore equal to the faradaic efficiency.

### 2.1.2 Cyclic voltammetry

Cyclic voltammetry is an electrochemical method with which the behavior of an analyte regarding voltage dependence can be studied. The voltage changes linearly with time and cycles between two voltage set points. The current at the working electrode associated with the voltage change is plotted against the voltage and shows an analyte dependent shape as an electrochemical spectrum. Dependent on the voltage the measured current can be traced back to faradaic, capacitive or adsorption parts [6]. Figure 2.1 shows a CV of a gold mesh 2.25 cm²

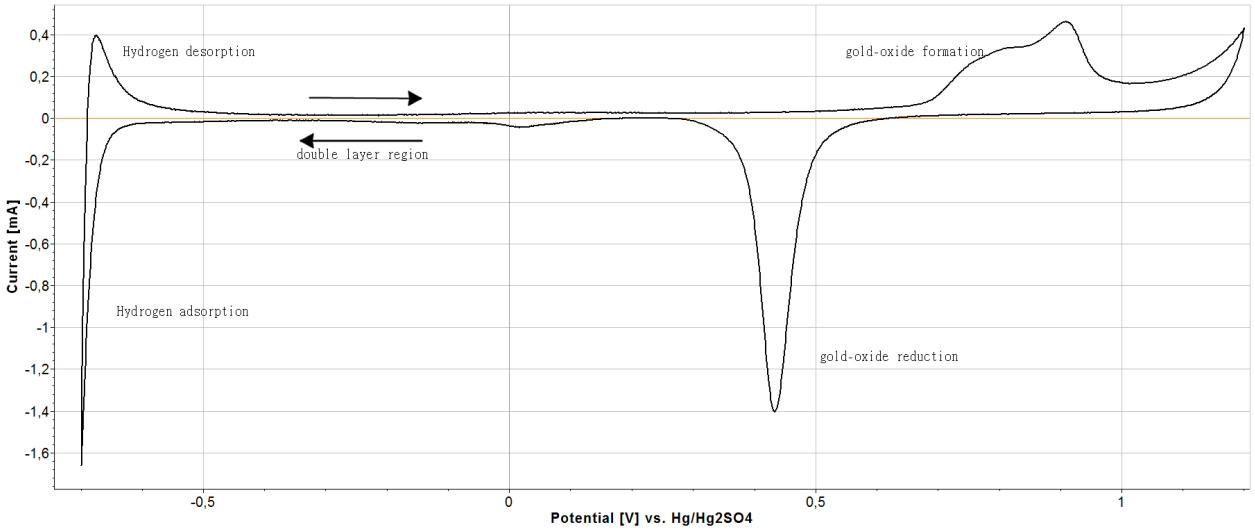


**Figure 2.1:** Cyclic voltammogram of a polycrystalline gold electrode in 0.5 M $H_2SO_4$

in 0.5 $H_2SO_4$ with a scan rate of 100 mV/s. As counter electrode a similar gold mesh was used and the reference electrode was a saturated Mercury/mercury sulphate ($Hg/Hg_2SO_4$) electrode. Argon was flushed continuously in the one-compartment cell. The specific reaction regions are clearly visible. In the cathodic region the hydrogen adsorption and desorption peaks are distinctive and in the anodic region oxide-formation is visible. The oxygen-reduction peak gives information about the amount of oxide that was formed and can be used to, for example, extract the electrochemical surface area of the electrode. Figure 2.2 shows a CV of a gold mesh 2.25 cm² in 0.1 M $KHCO_{243}$ with a scan rate of 100 mV/s. The cell conditions are similar to the one with sulphuric acid before. The specific reaction regions are clearly visible. Hydrogen adsorption and oxide-formation are still clearly visible but the oxygen-reduction peak and hydrogen desorption are less distinctive.

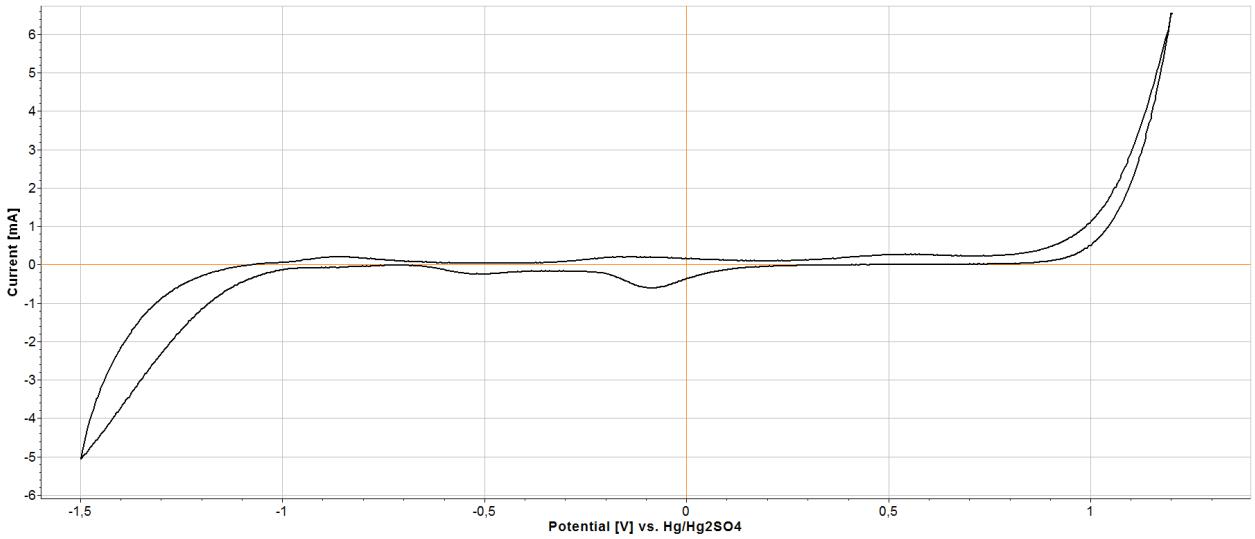


**Figure 2.2:** Cyclic voltammogram of a polycrystalline gold electrode in 0.1 M $KHCO_3$

### 2.1.3 Evaporation

Au-samples as a base for production of porous gold electrodes were prepared by thermal deposition in vacuum by Björn Wickman(Supervisor). $Au$ was deposited on a Si-wafers to produce a thin Au-film with a roughness factor of 1.12 and a nominal thickness of 100 nm.

### 2.1.4 Fabrication of NPG film electrodes

Electrochemical deposition of gold on a metal substrate can be achieved by applying a cathodic potential on an substrate in the presence of gold ions in aqueous solution:

$$Au^{3+}(aq) + 3e^{-}ßAu(s) \tag{2.11}$$

For gold a suitable source is $AuCl_3$ in 0.5 M $H_2SO_4$ solution. $AuCl_3$ dissolves to $Au^{3+}$ ions and $Cl^{3-}$ cations in solution. A cathodic potential will deposit gold on the gold electrode and at the same time hydrogen evolution reaction (HER)takes place. NPG electrodes can be fabricated electrochemically as well. The group of Arvia [7] presented a method in 1994 that is based on the reduction of hydrous gold oxide layers by using a fast periodic potential routine in 0.5 M $H_2SO_4$ solution. The oxide layers are prepared by applying a periodic symmetric square-wave potential scheme in the anodic potential region at 5 kHz (0.45 V - 2.7 V vs. SHE). This AuO layer is then reduced by scanning from 1.5 V to somewhere in between 0.05 V and 0.95 V at different sweep rates. The result was a columnar structured rough gold film of several nm depth. A different method was presented by Zhang at al. [8] in 2007. The group deposited a Zn-$Au$ alloy on a plane gold electrode in ZnCl2/BA electrolyte and de-alloyed it again while producing a nano structured layer on the surface. Then Zn was deposited again on the nano structure and stripped off again. After several cycles the group produced a NPG electrode. In this work a mixture of these methods is used to prepare NPG electrodes. A plane 100 nm $Au$ film is evaporated on a silicon wafer in order to give a conductive substrate. On top of this $Au$ film gold is electroplated by applying a linear multicyclic electrochemical alloying/dealloying process between 1 V vs. SSE down to -10 V vs. SSE. In the anodic part an oxide layer is formed on the surface and reduced again. In the cathodic region gold is deposited with hydrogen evolution reaction occurring at the same time. This method increases the surface area and establishes a

porous layer of gold on the silicon wafer. It is possible to control the increase of electrochemical surface area by limiting either the number of cycles or by lowering the cathodic potential limit. After each cycle the increase of peak area is visible compared to the last cycle since the reduction peak of the oxide layer in the anodic potential region changes. This change can be taken for an estimation of the surface area increase. A lower cathodic potential increases the current. The experimental results showed that this current raise increases the surface area significantly. This might be due to interaction of hydrogen evolution with the surface but is not further studied here. The method is further explored and the successful use is demonstrated in section 3.5.2.

## 2.2 Explanation IR-Drop and methods

The potentiostat used in electrochemical measurements controls and measures the voltage difference between the input and output of the potentiostat in relation to a reference electrode system. Thus, it accounts for the voltage drop of the entire electrochemical system. Sources of the voltage drop are the ohmic resistances and impedances in the wires, electrodes and electrolyte. The point of interest which is important for the electrode reactions is the potential drop across the electrode surface on the solution side of the double layer. This potential drop consists of the double layer capacitance $C_f$ and a resistance due to charge transfer across the interface (see [4]). This potential cannot be set and measured directly but the potentiostat accounts for sources of voltage drops and sets the voltage of the counter electrode accordingly. A problem of an uncompensated voltage drop occurs due to the nature of the reference electrode. The user sets the desired voltage at the working electrode relative to the reference electrode. This implies that the standard potential between the working electrode and the reference electrode is known (OCV) and that it is not current dependent. Current independence is only possible if the reference point is directly located at the surface of the electrode, what is impossible in practice, since one has to account for resistance in the electrolyte, the connectors and from interfaces like the surface film. The uncompensated voltage drop follows ohm's law in most cases: $\Delta V_{IR} = I_{cell} \cdot R_u$ with $R_u$ termed the uncompensated cell resistance between the working electrode and the reference electrode and $I_{cell}$ being the cell current measured by the potentiostat [9]. In this case $R_u$ can be determined by using an AC current at high frequencies which will be describe below. There are different ways to avoid the appearance of IR-Drop problems. What was already mentioned is the distance between the reference electrode and the working electrode. By working with a Luggin capillary this distance can be minimized and so will be $R_u$. $R_u$ is also dependent on the material in this case the electrolyte composition. A less conductive electrolyte will increase $R_u$ and therefore increase the error in the measurements. Using a more conductive base electrolyte (higher molarity) or a supporting electrolyte could reduce the influence of the uncompensated voltage drop. In chapter 2.3 the dependence of the electrolyte in terms of purity and pH will be discussed with the conclusion that a supporting salt will interfere with the surface chemistry and thus with the reactions and so does a different pH. Fujishima et. al. investigated the changes by adding different supporting electrolytes. [10] Their conclusion was that the supporting electrolyte changes the product selectivity of the used copper electrode. Therefore, $R_u$ cannot be reduced by adding a support or changing the electrolyte concentration. A last method is connected to the cell current. The number of surface reactions is dependent on the surface area. A low surface area will reduce the total number of reactions and therefore lower the total current without changing the surface reactions [11].

If it is not possible to lower $R_u$ up to a negligible value, the exact value of $R_u$ has to be measured in order to correct mathematically. Measurements techniques are based on either Direct Current (DC) and Alternate Current (AC). An AC technique is Electrochemical Impedance

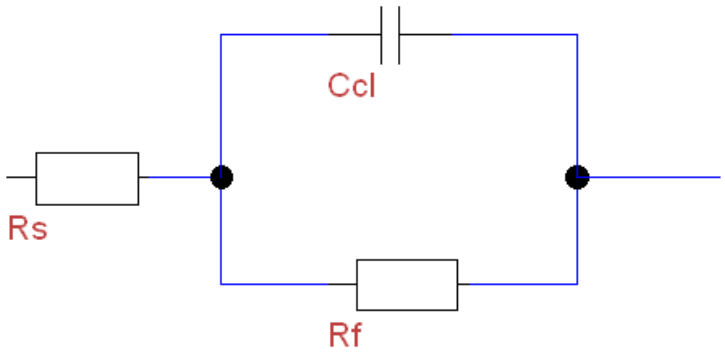


**Figure 2.3:** Randle's cell model: $R_s$ is the electroctolyte resistance. $C_cl$ the double layer capacity in parallel with the charge transfer reactioncharge transfer reaction $R_f$

Spectroscopy (EIS) [12] which measures the impedance of the cell as a function of frequency of the AC current. If the ohmic drop has no impedance, thus it is truly an ohmic resistance, the equivalent circuit, Randle's cell model (Figure 2.3), of such a system shows $R_u$ or $R_s$ in series with the impedance of the cell reaction. In this case a scan with AC with different frequencies will reveal $R_u$, since the capacitor will act as short circuit. For lower frequencies the impedance will consist of $R_u$ and $R_f$, for higher frequencies the current passes without resistance through the capacitor and the only resistance visible is $R_u$ (see figure 4.2 on page 37). The value for$R_u$ can be read from the Nyquist-diagram, which shows the resistive impedance on the x-axis and the reactive impedance on the y-axis with the frequency as a parameter going from high values (right hand side) to lower values (left hand side)(see figure 4.1 on page 36). . With higher frequencies $R_u$ will be the only impedance being measured and an intersection with the x-axis is visible. The point of intersection represents the $R_u$ value, if Randel's cell model is valid for the investigated cell system. For this simple case, $R_u$ is rather easy to determine with one single PEIS measurement before the measurement series. If Randel's cell model is not valid and for example the cell shows inductive behaviour (negative imaginary axis at high frequencies), the determination of $R_u$ is more difficult. [13]

## 2.3 Electrochemical Surface Determination

In order to estimate the quality of an electrode parameter like the electrode reaction rate, knowledge of the surface area is needed. The surface can be described in two essential ways. One is simply measuring the projected surface area of the electrode, which is defined by the projection the area on a plane. When an electrode has a complicated microscopic surface structure with porous layers the projected surface area is not appropriate. What matters are the electrochemical sites participating in the reaction process. For appropriated comparison of the behaviour of the electrode, knowledge of the reaction rates per unit surface area are needed. The real surface area can be given per unit projected surface area and is called roughness factor. [14]

$$f_r = A/A_g \tag{2.12}$$

where A is the real surface area and $A_g$ the projected surface area. In this work different techniques for real surface area determination were used to determine the electrochemical surface area of NPG films). For a review see Trasatti et al. [14]. The techniques used in this work are based on the double layer capacitance ratio, underpotential deposition of copper ions and

oxygen adsorption.

### 2.3.1 Double layer capacitance ratio

The double layer capacitance can be measured by determining the total charged passed when no reactions are taking place. Comparing two electrodes of the same material and under the same conditions the division of the total charge can offer an estimation of the surface area ration. If the surface area of one electrode is known it is possible to roughly determine the surface area of the other electrode. This method has several limitations and can only be an estimation. For more information see [14]. Whereas capacitance measurements are very reliable on planar gold, Rouya [15] encountered a factor 1,5 - 1,75 larger surface area on NPG compared to other measurement techniques what suggest that double layer capacitance measurements are less reliable for NPG.

### 2.3.2 Underpotential deposition of Copper ($Cu$ UPD)

Metal ions can be used to determine the surface area if a monolayer coverage can be established and if the charge associated to the metal adsorption is known. Metal ions in solution are attracted to cathodic electrodes. The deposition can be divided into Bulk deposition and monolayer formation [16]. For monolayer coverage the charge measured by the potentiostat can directly be referred to the real surface area of the electrode. In order to determine the surface area the cathodic current is integrated over time what gives the accumulated charge associated to the $Cu$ Underpotential deposition (UPD). In a $Au/Cu$ system the desorption charge associated with copper ions is between 240 to 455 $\mu$Coulomb / cm$^2$ and is dependent on the plane orientation of the gold surface [17],[18], [19]. Here one has to account for double layer charge in the monolayer formation region and for charge contribution from the oxygen reduction reaction. As a source for copper ions Copper sulphate ($CuSO_4$) can be used in small concentration as an additive to the electrolyte. A procedure of UPD for copper on gold was presented by Schultze in 1976 [17] and recently by Rouya [15]. Rouya used a $Cu$ UPD charge of $0.420 mC/cm^2$ for a smooth polycrystalline $Au$ electrode in $1 * 10^{-}3$ M $CuCO_4$ solution in 0.5 M $H_2SO_4$ within a potential range of -0.12 V to -0.44 V vs MSE. A problem with this method is the unknown cathodic potential-limit of the monolayer formation. If the cathodic voltage is too high, bulk deposition occurs but the calculation method is only valid for a monolayer coverage and surface transformation cannot be excluded anymore. In fact this method gives the number of active sites on the electrode. If there are large deactivated sites on the surface, the calculated area can be very different from other methods. Another problem occurs if the plane orientation of the surface is unknown. Although potentiodynamic desorption spectra (Current vs. electrode Potential) are known for certain planes, one cannot trace back from the spectra to the plane surface. Thus, without knowledge of the surface structure this method can only be an approximation.

### 2.3.3 Oxygen adsorption

At higher anodic Voltage oxygen adsorption takes place in aqueous solutions. Similar to $Cu$ UPD and depending on the voltage a monolayer or multilayer coverage of chemisorbed oxygen on a metal surface can be used to determine the real surface area. Oxygen is adsorbed in the anodic sweep of a cyclic voltammetric experiment and it is stripped off in the cathodic sweep, giving the characteristic cyclic voltammogram of gold. If the monolayer region for a polycrystalline $Au$ surface is known the anodic charge associated to polycrystalline $Au$ electrodes is

about 386 microC [20]. Thus, a bilayer is associated to a charge of 0.772 $\mu\ C/cm^2$ [21]. As a rough estimation the charge ratio between two oxidation peeks can be used to determine the surface area ratio of two electrodes [14]. The procedure was recently presented by Rouya [15]. The group used 0.05 M $H_2SO_4$ electrolyte solution and performs cyclic voltammetry at 100 mV/s.

## 2.4 Electrochemical reduction of $CO_2$

The process of electrochemical reduction can essentially be considered as a fuel cell process running in reverse. $CO_2$ that is flushed into an electrochemical half-cell is reduced at the cathode in the presence of an electrolyte to different products. The electron needed for the reduction comes from the anode where the oxygen evolution reaction (OER) takes place. In order for the Oxygen evolution reaction (OER) to take place, a potential is induced, i.e. energy is supplied, between the counter electrode and the working electrode. The first report about electrochemical reduction of $CO_2$ is dated from 1985 by the fundamental work of Hori. [22] Hori discovered the unique properties of a copper electrode to synthesize hydrocarbons from $CO_2$ with rather high current densities and current efficiencies in the expense of a rather low selectivity for single hydrocarbons. In fact, Hori discovered a broad range of hydrocarbons formed.

### 2.4.1 Reaction products

Among hydrogen ($H_2$) from the Hydrogen evolution reaction, carbon monoxide ($CO$) and various hydrocarbons like methane, ethane, propane, methanol, ethanol and more complex compounds like formate or glyoxal are produced. The half reactions for the major products on noble metals like copper, silver or gold are listed with its standard potentials below.

$$\begin{aligned} 2H + +2e^- &\rightarrow H_2 \\ CO_2 + 2H^+ + 2e^- &\rightarrow CO + H_2O \\ CO_2 + H^+ + 2e^- &\rightarrow HCOO \\ CO_2 + 8H^+ + 8e^- &\rightarrow CH_4 + 2H_2O \\ 2CO_2 + 12H^+ + 12e^- &\rightarrow C_2H_4 + 4H_2O \end{aligned}$$

The products formed can also be produced by homogeneous catalysis, heterogeneous catalysis, photo catalysis or photo-electrochemical reduction. The later reduces carbon dioxide with the energy of incident natural or artificial light. The benefit of electrochemical reduction is the possibility of using excess energy from renewable energies in order to store it as chemical energy in the produced hydrocarbons. The choice of the electrode material has a significant impact on the selectivity of the products. The electrode materials serve as a catalyst and are selective for certain reactions. In aqueous solution there can be 4 different kinds of electrode groups distinguished which are based on the main product that is synthesized in the reduction process.

### 2.4.2 Electrodes and electrolytes

Different electrode materials have different properties when it comes to $CO_2$ reduction.Table 2.3 gives an overview of the major products of different electrode materials. Where $Hg$, $Cd$, $Pb$,

| Chemical | Formula | electron transfer | Equilibrium Voltage [V] | phase |
|---|---|---|---|---|
| Formate | COOH | 2 | -0.02 | Liquid |
| Carbon monoxide | $CO$ | 2 | -0.10 | Gaseous |
| Methanol | $CH_3OH$ | 6 | 0.03 | Liquid |
| Glyoxal | $C_2H_2O_2$ | 6 | -0.016 | liquid |
| Methane | $CH_4$ | 8 | 0,17 | Gaseous |
| Acetate | $CH_3COO - M^+$ | 8 | -0.26 | liquid |
| Glycolaldehyd | $C_2H_4O_2$ | 8 | -0.03 | liquid |
| Ethylene glycol | $C_2H_6O_2$ | 10 | 0.20 | liquid |
| Acetalaldehyd | $C_2H_4O$ | 10 | 0.05 | liquid |
| Ethanol | $C_2H_6O$ | 12 | 0.09 | liquid |
| Ethylene | $C2_{H4}$ | 12 | 0.08 | Gaseous |
| Hydroxylacetone | $C_3H_6O_2$ | 14 | 0.46 | liquid |
| Acetone | $C_3H_6O$ | 16 | -0.14 | liquid |
| Allyl Alcohol | $C_3H_6O$ | 16 | 0.11 | liquid |
| Propionalaldehyd | $C_3H_6O$ | 16 | 0.14 | Liquid |
| 1-propanol | $C_3H_7OH$ | 18 | 0.21 | liquid |

**Table 2.2:** Standard reduction potentials at pH 6.8 taken from [23]

| Group | Elements | Major product |
|---|---|---|
| I | Pb, Hg, In, Sn, Cd, Tl | HCOOH |
| II | Au, Ag, Zn, Pd, Ga | CO |
| III | $Cu$ | Hydrocarbons |
| IV | Pt, Ni, Fe, Ti | $H_2$ |

**Table 2.3:** Major products of $CO_2$ reduction for different electrodes out of different elements

$Tl$, $In$, $Sn$ mainly produce formic acid, and Zn, $Au$ and Ag mainly produce carbon monoxide. Copper has as already mentioned in the introduction the unique property to synthesis hydrocarbons, aldehydes and alcohols. Other metallic materials like $Al$, $Ga$ and group VIII elements (but $Pd$) do not catalyse carbon dioxide reduction. In the list of reactions above the Hydrogen evolution reaction (HER) is mentioned although $CO_2$ is not the reactant. In fact HER is a side reaction occurring on almost all kinds of electrode materials but they are dominant in the 4th group ($Pt$, $Ni$, $Fe$, $Ti$) [24].

The performance of an electrochemical cell to conduct electrochemical reduction of $CO_2$ is dependent on several parameters. On one hand, the conductivity of the electrodes and the electrolyte are important for the current density for example. On the other hand, highly active and long lasting catalyst layers are necessary for stability and thus economic reasons. Another important aspect is the mass transport of the products from the catalyst layers to the electrolyte in order not to block the reduction process at the working electrode. The same

applies for the counter electrode where thick layers of gold oxide can be a limiting factor in the oxygen evolution reaction. The choice of the working electrode and its manufacturing determine the surface structure and its activity towards $CO_2$ reduction. The performance of the electrochemical cell can be determined by calculating the faradaic efficiency of the products, the energetic efficiency of the entire cell and the current density of the electrode.

### 2.4.3 Reaction intermediates

The end products of $CO_2$ reductions are easy to analyse by in-situ applied analytical methods. The formation of these products on the catalytic material in contrast is not easy to analyse. Researches on the formation process suggest that there are key intermediates involved in the reduction and that reaction briers are the reason for rather high overpotentials. The formation process from an energetic (DFT) and microscopic perspective for copper and gold is discussed later in section 2.4.5 and 2.4.5 . A key intermediate in the reaction to hydrocarbons appears to be CO.

### 2.4.4 Reaction parameters

The reaction process of electrochemial reduction of $CO$ is complicated and not completely understood. What is well known from experiments is the reaction dependence on several parameters like electrode potential, PH-value and $CO_2$ concentration as well as mass transport and pressure.[25]

#### Electrode Surface structure

The importance of the electrode material was already carried out. Another important parameter is the surface morphology of the electrode. The surface of a metal electrode can be described by its crystal structure. This refers to the arrangement and orientation of atoms into a crystal lattice throughout the material. The different crystal structures are named after the Miller Indices. Hori at al. [26] published in 2003 an experimental study of various crystal structures of single crystal copper electrodes. In his experiments he proved that on $Cu$ [111] facets methane is produced instead of ethylene which is dominant on the [100] facet. He concludes that the surface orientation has a great influence on the selectivity of the reduction process. He explains the differences with the presence of various steps and kinks on the electrode surfaces. On a macroscopic level the adsorption of molecules in solutions takes place on the sites of the surface. There are different kinds of sites that are distinguished by the number of surface planes that surround an adatom on the surface. [27].

#### PH-dependence

A main reaction accompanying the reduction process is the Hydrogen evolution reaction. H+ ions are adsorbed to the electrode surface to generate gaseous hydrogen. The H+ presences alters the pH close to the surface to more acidic states and is due to mass transport phenomena different from pH of the bulk solutions. On the other hand the reduction of Water and $CO_2$ to hydrocarbons involves the formation of hydroxyl ions which have an alkaline influence on the pH. (Self-dissociation of water and $H^+$ as reactant with $H^+$). Chemical reactions involving $H^+$ and $OH^-$ are normally pH dependent and thus the surface pH is an important parameter for the overall reaction. The local changes due to the formation of $H^+$ or $OH^-$ are meant to

be buffered by the choice of the electrolyte and its concentration. An electrolyte is a buffer solution if an addition of a strong acid or base does not change the pH of the solution notable.

$$HCO_3^- + OH^-$$

$\rightarrow CO_3^- + H_2CO_2$ undergoes several equilibrium reaction when in contact with a $KHCO_3$ electrolyte solution. The reactions are dependent on the pH and thus in the concentration of $KHCO_3$. Above pH 7.4, which is about 0.45 M $KHCO_3$ dissolved $CO_2$ mainly reacts with the predominant Hydroxyl ions in the slightly basic solution.

$$CO_2(aq) + OH^- = HCO_3^-$$

Below pH 7.4 $CO_2$ reacts also with water to $H_2CO_3$ what dissociates to a bicarbonate ion and a proton. The more acid the solution, the more dominant is this reaction:

$$\begin{aligned} CO_2 + H_2O &\rightarrow H_2CO_3 \\ H_2CO_3 &\rightarrow HCO_3^- + H^+ \end{aligned}$$

In fact in Gupta et al. [28] showed the influence of electrolyte concentration on the reduction process on the electrode. The conducted concentration calculations close to the surface area by applying diffusion calculations in a $KHCO_3$-$CO_2$ system while taking into account surface reactions. Their results suggest that the pH close to the surface is higher compared to the bulk solution when the cathode is polarized and the reaction takes place and the differences increase with increasing current. The result is not surprising since $CO_2$ reductions produces besides of product molecules always OH- ions at the electrode surface. It must be stated that the results are dependent on the diffusion conditions in the cell. A higher stirring rate will lower the pH differences but also decrease the diffusion of reactants to the surface. The group of Gupta continued with an analysis of electrolyte concentrations and surface pH from data of the group of Hori in 1989. Hori conducted $CO_2$ reduction experiments in a $KHCO_3$-$CO_2$ system with different electrolyte concentrations. Gupta analyses a "clear shift to less hydrogenated products with higher local pH [28]. A similar approach but with using a buffer solution was made by Shouten in 2012 [29]. The group compared the influence of 2 electrolytes, a carbonate buffer at pH7 and a NaOH electrolyte at pH 13 on two different copper facets [100] and [111]. Whereas on the [111] facets a higher pH seems to block hydrocarbon generation, on the [100] facet ethylene production starts at lower overpotentials at a pH of 13.

### Temperature dependence

Temperature dependence of $CO_2$ reduction was shown by Hori in 1986 [1]. Within a range between 0 °C and 40 °C $CO_2$ reduction was conducted in an electrochemical cell between -1.33V and -1.39V vs SHE. . A temperate drop caused a decrease in hydrogen evolution and an increase in methane production. A temperature raise resulted in a decrease of $CH_4$ production to about 5 % at 40 °C. The temperature influences several parameters of the reduction process. The $CO_2$ solubility is increased, reaction rates are changed and surface adsorption equilibria are changed. [24]

### Contaminations

Due to the fact that the reduction takes place at the surface of the catalyst and is thus adsorption dependent, any kind of impurity can differ or deactivate the catalytic activity of the

electrode. Several groups have reported problems with the reproducibility of results with the same electrode or stability problems for long time experiments. The group of DeWulf [30] reported in 1987 a drop of hydrocarbon selectivity from 65 % to 0 % faradaic efficiency within one hour. The electrode developed a black cover which was analysed to be graphitic carbon by X-ray photoelectron spectroscopy (xps) and Auger electron spectroscopy (aes). Carbon causes hydrogen evolution but does not reduce $CO_2$ to hydrocarbons. Since the copper sites are covered with carbon, $CO_2$ reduction is deactivated. The group suggests a side-reaction that synthesis carbon on the electrode surface from formate The group of Wasmus [4] encountered the same problem but within a much smaller timespan of 10 minutes. The group was able to regenerate hydrocarbon activity by anodic polarization which will be explained later in this chapter. In 2005 the group of Hori [31] summarized and analysed the reasons for contaminations. He postulates that there are three reasons for deactivation of electrodes: (1) Heavy metal contamination, (2) organic contamination, (3) poisoning by intermediated reactants of the reduction. The reduction of $CO_2$ takes place at the surface of the electrode. Molecules are adsorbed on the sites and interact with the near-field liquid phase to form hydrocarbons or hydrogen. The reduction takes place, evidently, in negative potential ranges. Metal ions attract to the negatively polarized electrode and deposit on the surface. The active sites may be blocked by these metal ions. Thus, the presence of metal ions other than the electrode material in the electrolyte may deactivate or alter the electrode activity and selectivity. For copper electrodes the result of contaminations can easily be seen. Since copper is the only element that reduces $CO_2$ to Hydrocarbons, metal impurities will decrease the selectivity for hydrocarbon synthesis. Organic contamination might come from water used for the electrolyte or are already present on the cell's surface. Surface active reagents may be adsorbed by the surface and deactivate the electrode. Kyriacou et al. [32] encountered deactivation of the electrode but could not trace the problem to surface contamination by doing XPS. Therefore they suggested that reaction intermediates or products that remain adsorbed on the electrode poison the hydrocarbon reaction. The stated reported experiments show the importance of an impurity free electrochemical cell. Less than one monolayer coverage of foreign metal atoms can deactivate an electrode. Thus, a purified electrolyte solution is evident in all catalyst dependent reactions, but in electrochemical reduction of $CO_2$, it is essential. Hori 2005 suggests pre-electrolysis of electrolyte solution as an appropriate method to remove metal contaminations of the solution. Electrolyte solutions even prepared from highly pure chemical reagents contain about 1.2 $\mu$M of heavy metals, mainly Fe and Pb,([31]) what is enough for a monolayer coverage. These small amounts of ions in solution are only detectable with atomic spectroscopy (etaas) methods but can by no means be neglected. Another explanation is a change of surface morphology on the electrode. As already indicated the surface structure is an important parameter that has an influence on the product selectivity. Chiacchiarelli et al. [33] made a study of Sn electrocatalysts showing degradation mechanism in cathodic regions in $KHCO_3$ electrolyte at rather high current density (175mA/$cm^2$). The group reports different kinds of surface morphology changes, i.e. grain etching, corrosion, deposit formation and black deposits. (see also [28] p.169) A way to avoid contamination is pulsed potential reduction [34] of $CO_2$ what was shown by Shiratsuchi 1993 [35]. This method did not deactivate the used copper electrode over hours but it should be stated that the pulse technique changes the conditions at the surface electrode and a steady state is not established. Other methods must aim on avoiding and removing of contamination. Prior to methods based on electrochemical cleaning the entire equipment should be cleaned. Swider-Lyons [36] provided a tutorial aiming on the development of preparation and measurement protocols for electrochemical experiments. The electrochemical cell, including glassware, stoppers, and o-rings, must be cleaned thoroughly of cationic, anionic, and organic

impurities to obtain reproducible measurements. He suggest cleaning the electrochemical cell with concentrated $H_2SO_4$ for 8 hours and rinsing it thoroughly with MilliQ water afterwards. The cell should then be boiled twice in MilliQ water. Electrolyte solution should be prepared from MilliQ water and chemical reagents that are as clean as possible.

#### Pre-Electrolysis

Hori 2005 [31] made a study with $KHCO_3$ electrolyte for $CO_2$ reduction with a copper electrode. The electrolyte was purchased from different manufactures. He compared the reagents with reduction series with and without pre-electrolysis. With the term "pre-electrolysis" an electrochemical technique is meant that has the purpose of reducing metal ions at an electrode surface by applying a cathodic current for several hours in order to remove contaminations thoroughly. The electrode should be removed while still kept cathodic in order to avoid redissolution in the electrolyte. His results showed clearly that the standard impurity levels of the reagents are too high for successful $CO_2$ reduction and that pre-electrolysis improves the results for reagents from all manufactures. Hori suggest a cathodic current of $2.5 * 10^{-}5A/cm^2$ with a Pt black cathode under an Argon atmosphere in the same electrochemical cell as the $CO_2$ electrolysis takes place. In another successful experimental study by Hori in 1987 on gold electrodes he gives a electrolysis current of $2 * 10^{-}2mA/cm^2$ [37] with $N_2$ gas bubbling for 20 h.

#### Anodic polarization

Wasmus et. al. [4] observed a loss of activity on their copper electrodes in 0.5 M $KHCO_3$ during reduction of $CO_2$. They saw a continuous blackening of the working electrode due to graphite deposition after several cathodic sweeps. The group was applying an anodic potential of -150 mV vs. SCE for less than one minute. This method is known as anodic polarization. The working electrode becomes the anode of the cell and molecules on the surface are stripped off. The group of Wasmus was able to recovers the metallic appearance of the electrode and also almost recover the catalytic activity of the working electrode.

### 2.4.5 $CO_2$ reduction on $Cu$ and $Au$

#### Copper Electrode

Copper has been demonstrated to be the only element to reduce $CO_2$ to hydrocarbons efficiently [28],[3]. The drawback is a large overpotential that needs to be applied in order to achieve these reactions. Figure 2.4 shows the results of Hori's group published in 1989 for a copper electrode in 0.1 M $KHCO_3$ at 19 °C. The results show that at low overpotentials Hydrogen formation is the dominant reaction but $CO$ generation is apparent even at -0.4 V vs. RHE. Hydrogen decreases constantly with higher overpotentials. $CO$ increases slightly and reaches a peak at about -0.8 V vs. RHE while almost disappearing at -1V vs. RHE. Ethylene and Methane production start at -0.7 V vs. RHE and -0.8 V vs. RHE. Those hydrocarbons make about 60% of the faradaic yield at -1 V vs. RHE. The equilibrium potential of $CH_4$ is +0.17 V vs. RHE and for C2H4 it is +0.08 V vs. RHE but the reaction to hydrocarbons requires a potential of about -0.7 V vs. RHE. The reason for this behaviour is not well understood. It is beyond understanding how copper catalyses hydrocarbons and why there is such a large overpotential. These questions do not only count for the copper electrode but for catalysts in reduction of $CO_2$ in general. The group of Norskov [38] tried to explain this unique behaviour with Density

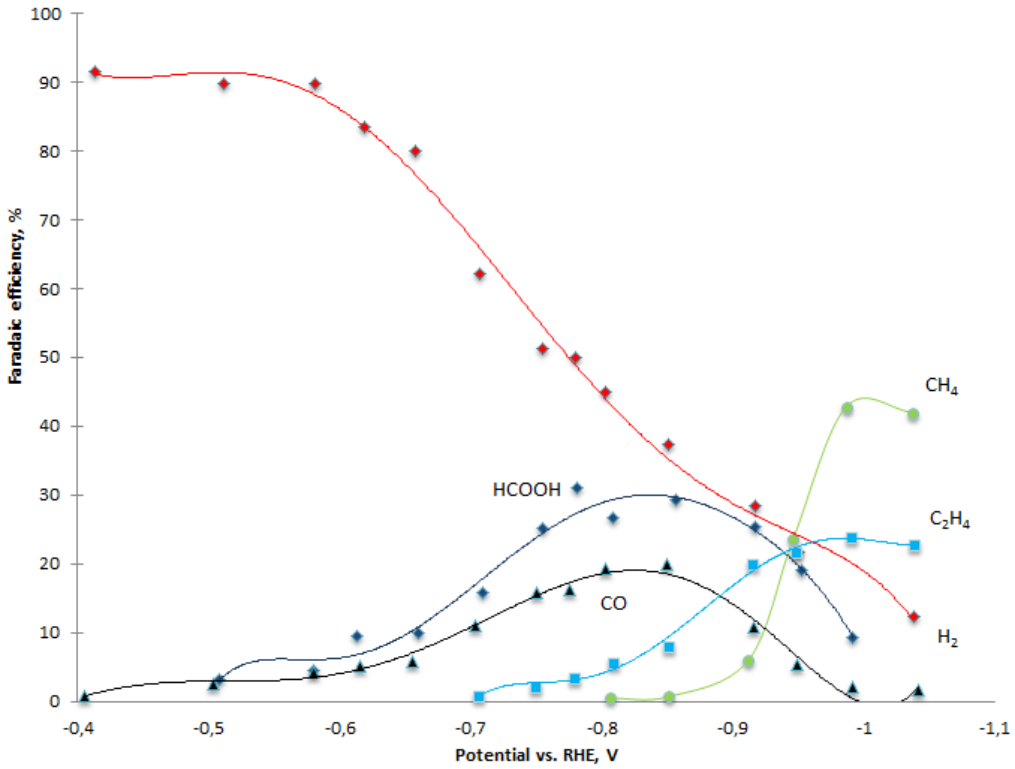


**Figure 2.4:** Faradaic efficiencies of reduction products plotted against potential vs. RHE for the electrochemical reduction of $CO_2$ at a copper electrode in 0.1 M $KHCO_3$(pH 6.8) at 18.5 °C, taken from Hori et al.[3] in 1989.

functional theory (DFT) calculations, a schematic representation is visible in figure 2.5. The group modelled a computational hydrogen electrode combined with DFT and applied it to a copper [211] facet. Their calculations match to the results of Hori. According to Norskov, the high overpotential needed to enable a first reduction pathway comes from oxidation of the copper step sites which goes along with OH and Oxygen adsorption on the surface. A voltage of -0.3 V vs. RHE is needed to "clear" the sites and entitle $H_2$ evolution. The second pathway is formation of formic acid, which requires a voltage of -0.41 V vs. RHE according to the model. $CO_2$ and a proton-electron pair ($H^+ + e^-$) is adsorbed as a carboxyl species COOH to the surface where it forms formic acid by reacting with another proton-electron pair. $CO$ as the third pathway is also synthesized from the carboxyl group but the reaction with the proton-electron pair splits water from the molecule and leaves $CO$ as a loose molecule at the surface. The next pathway opens up hydrocarbon formation and evolves directly from $CO$ creation. $CO$ reacts with Hydrogen and forms COH (Hydrogenation) A second proton-electron pair adds to form formaldehyde ($H_2CO$) and protonation with water at the surface forms adsorbed methoxy ($O - CH_3$). A proton from dissociated water reacts now with the methyl group to $CH_4$ which completes the pathway to form hydrocarbons. Another interesting analysis from the model explains the decrease of current density at -0,8V vs. RHE in Hori's results. It suggests that the copper surface is covered with $CO$ which blocks the active sites. A higher voltage clears the surface and increases the current density again. These pathways of reactions were supported, with many others, by Hori in 1998

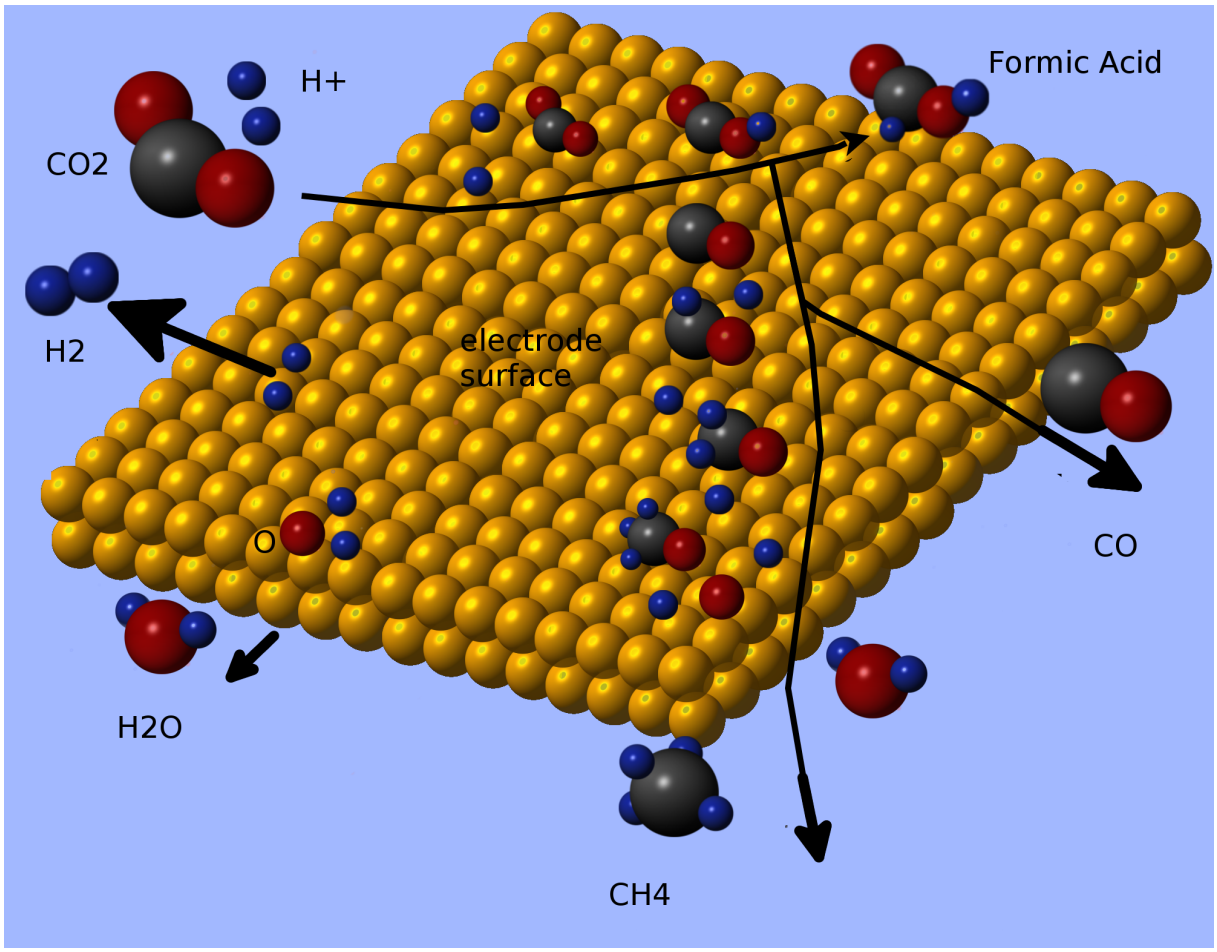


**Figure 2.5:** schematic represetation of the pathways of $CO_2$ reduction suggested by Nørskov et al. [38]

### Gold electrode

Gold electrodes predominantly synthesize carbon monoxide from $CO_2$. The theoretical equilibrium potential of this reaction (Formula Number) is -0.52 V vs SHE at pH7 and 25 °C [37]. Hori reached in 1987 a $CO$ current efficiency of 77 % at -0.8 V vs. SHE in 0.5 $KHCO_3$ with a pure gold wire. [37] A recent development is the use of NPG films that have been understood to enhance the catalytic activity of gold. The group of Kanan et al. [2] reported in 2012 an overpotential of only 0.14 V with a current density of 0.3 – 0.5mA/cm$^2$ and 65 % FE for $CO$ in $CO_2$-saturated 0.5 M NaHCO3, pH 7.2 % on a nanoporous gold film with a roughness factor of 72 (Figure 2.6). The group used a method presented by Vela in 1994 [7]. They reduced $Au$ oxide films to create $Au$ nanoparticles on the electrode. During 8 h electrolysis the electrochemical surface area decreased to a roughness factor of 17 which was explained with sintering of the surface. Today's major problem is that there is either a high selectivity for a certain product (e.g. $CO$ on gold) or a high current density. But both combined is needed for an efficient electrochemical cell. In summary the major obstacle for an efficiency electrochemical reduction of $CO_2$ today is a lack of a catalyst material that on hand lowers the overpotential and also achieves high selectivity and current densities. Thus, slow kinetics on the cathode side at low potentials has to be surmounted. It is also not well understood what factors are essential for the consideration of a catalytic material. There are studies of the surface morphology that show that the electrode structure might be a key to find a solution. Furthermore there is a lack

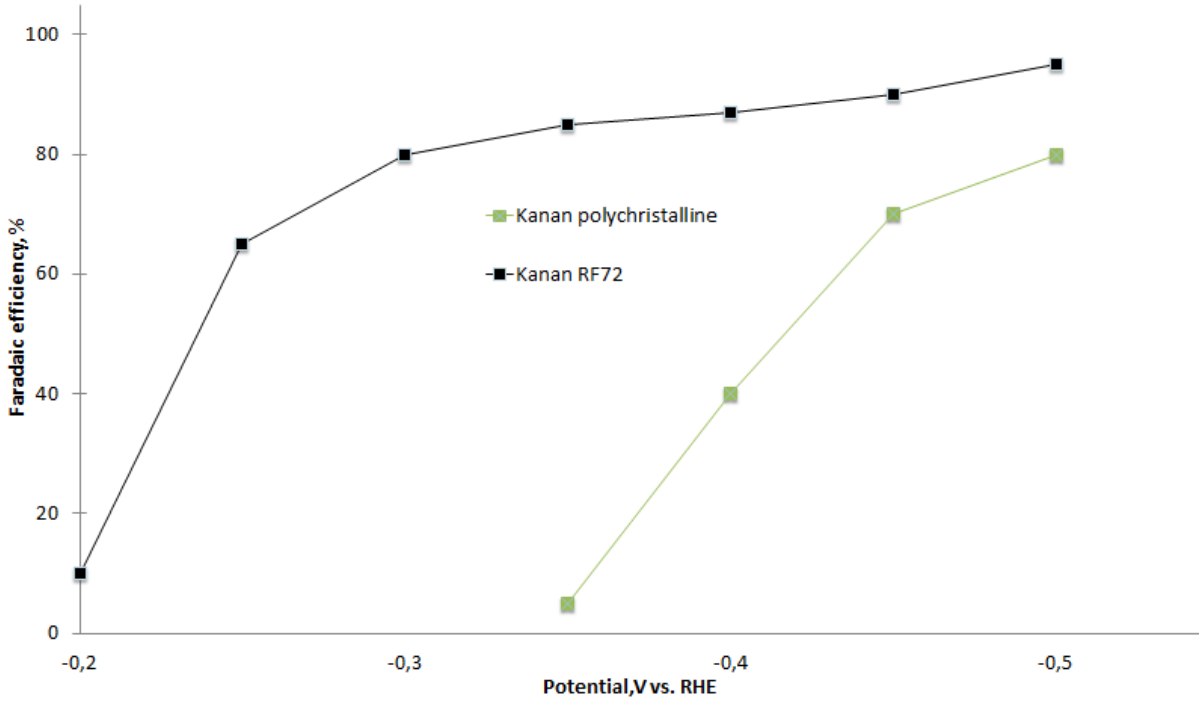


**Figure 2.6:** Results of $CO_2$ reduction from Kanan et al. [2] on a nanoporous gold electrode (RF72) in 0.5 $NaHCO_3$

of knowledge about the possibilities to drive the selectivity of the reduction process. Gaseous and liquid products may cause interactions with the reduction processes. It is known that the near-field volume on the electrode surface is of great importance. Products formed and adsorbed on the electrode surface block active sites. The progress in catalyst research for $CO_2$ reduction is due to the lack of theoretical understanding of the reduction process dependent on experimental data.

# 3

# Methods and experimental work

In this chapter the set-up and the methods are described. The calibration of the set-up including volume determination and devices calibration is explained. Electrode treatment and preparation as well as surface area determination and electro deposition of gold is presented.

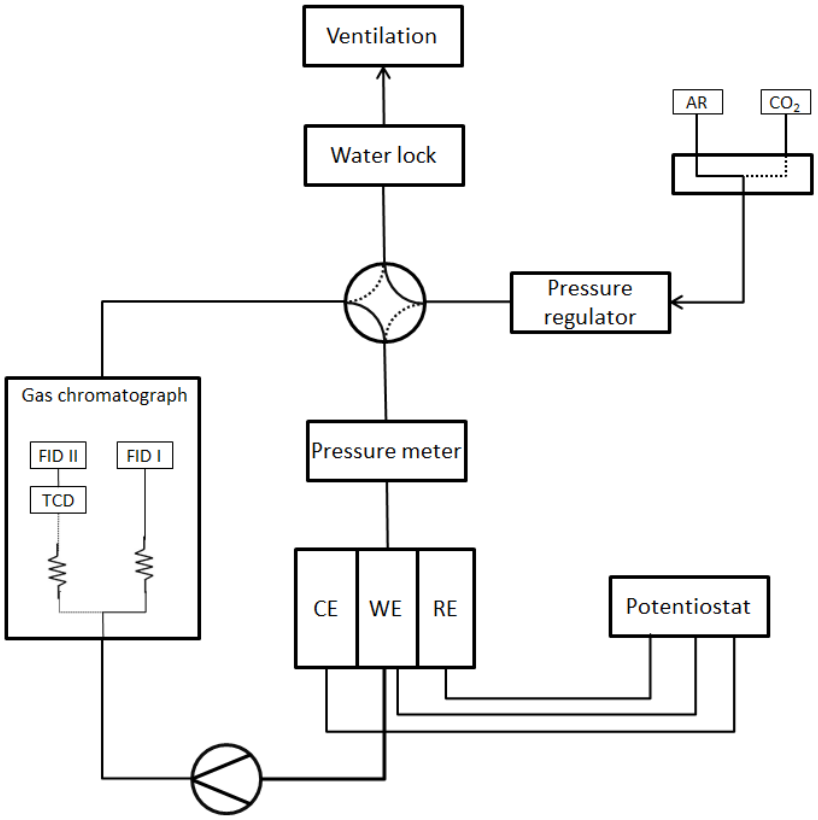


**Figure 3.1:** Schematic view of the experimental set-up. The electrochemical cell is displayed with three compartments consisting of CE=Counter electrode; WE=Working electrode and RE=Reference electrode. Different pathways possible due to valves are displayed with dotted lines.

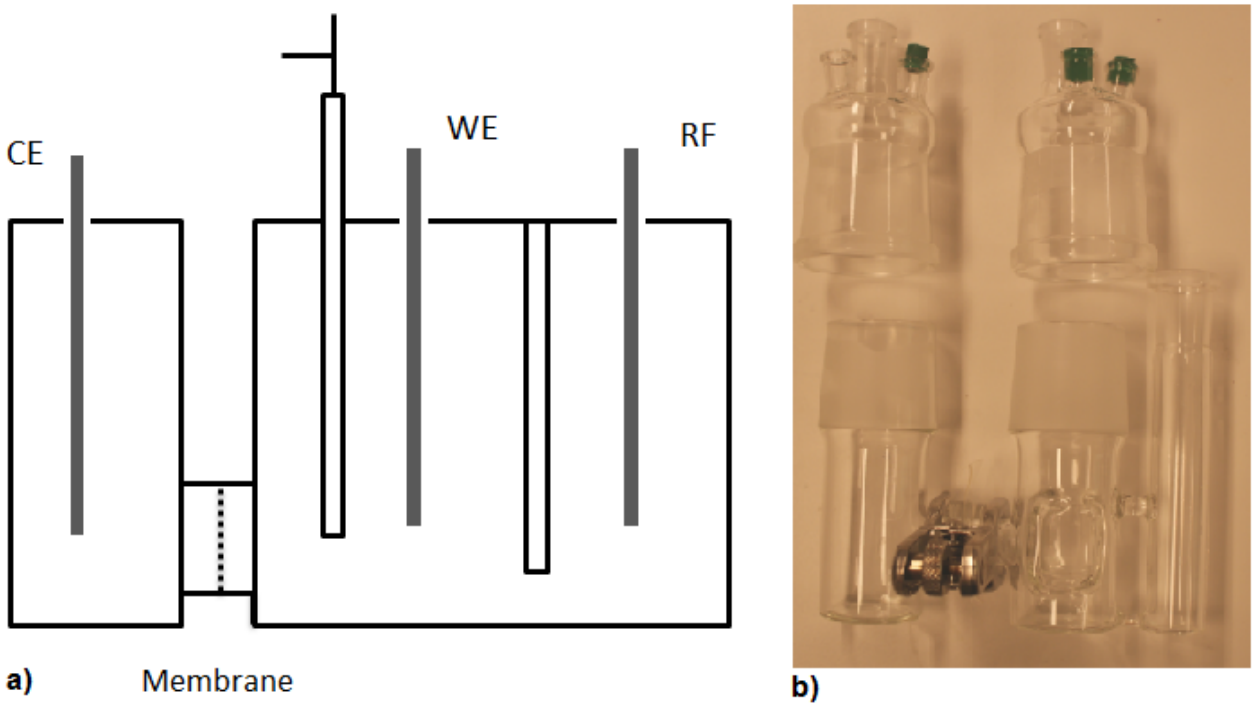


**Figure 3.2:** Schematic view a) and picture b) of the cell for electrochemical reduction of $CO_2$.

## 3.1 Experimental set-up

$CO_2$ reduction is conducted in a set up consisting of an electrochemical cell supplied by an potentio-galvanostat, a gas chromatograph ($GC$) to analyse the products of the reaction in the cell and additional equipment like pressure meter, pressure controller, a pump, a three way valve, a four way valve and connecting tubes. The three way valve directs either $CO_2$ or Argon in the tube system. A pressure regulator determines the flow speed. The four-way valve controls the direction of the gas flow. Either the input stream is directed to the ventilation ($vent$) via a water lock or to the experimental loop, i.e. the cell and the GC. When the input flow is directed to vent the tube system is closed and the gas inside circulates in the loop. In the experimental loop the gas flow passes a pressure meter after the 4-way valve before it bubbles into the electrolyte in the working electrode compartment of the cell. The gas volume above the electrolyte is captured and passes a liquid pump before it goes through the GC. Afterwards the gas stream goes again to the 4-way valve and flows, depending on the settings, either to the ventilation or cycles in the tube system. The schematic view is shown in Figure 3.1.

### 3.1.1 Cell and electrodes

The electrochemical cell consists of three compartments hosting the Working electrode (WE)the Counter electrode (CE) and the Reference electrode (RE). A picture and the schematic view are visible in figure 3.2. The set liquid volume for counter electrode compartment is 20 ml, for the working electrode compartment, 25 ml and for the reference compartment 2.5 ml in order to have a similar filling level. Working electrode and counter electrode compartment are separated with a PE-Membrane and connected and sealed with a detachable flange. Gas is flushed into the working electrode compartment through a two-way gas bubbler. The gas is injected in the liquid and leaves the compartment through the bubbler opening in the cap of the cell. The cell was designed and built at the Technical University of Denmark in a prior project. Figure 3.3

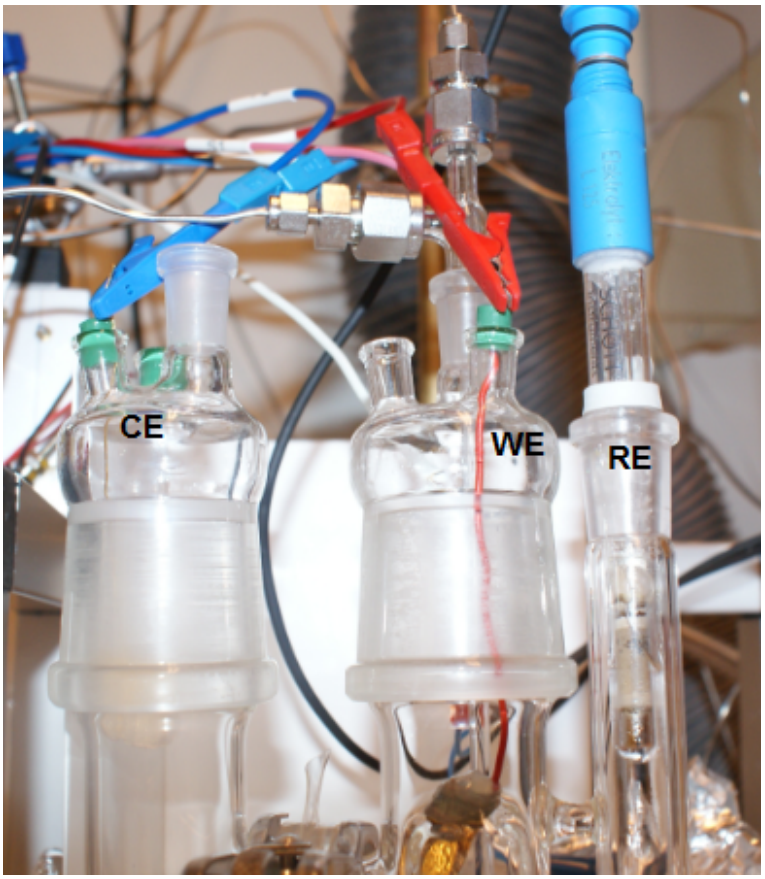


**Figure 3.3:** Picture of the cell with connections to gas loop and potentiostat

shows the cell with electrodes and connections to the potentiostat and the gas loop.

### 3.1.2 Reference electrode

As reference electrode a $K_2SO_4$ saturated mercurous sulphate $Hg/Hg_2SO_4$ electrode (MSE) from *SI Analytics* is used with a potential vs. NHE (25 °C) of +0.650 V.

### 3.1.3 Devices and Equipment

Gaseous reaction products are captured in the closed tube system and directed to the gas chromatograph. The gas chromatograph is an *Agilent 7890A* with an adapted column system with the purpose of separating the gas flow into two streams. When a measurement is started, the valves of the GC turn on and capture a sample of the gas stream. Inside the GC a two column set up is used for separation of different reaction gases. The gas stream goes through the first column where it is As mobile phase Argon is used. 3 different detectors and a nickel catalyst are used as detection components. Two Flame ionization detector (FID) with Hydrogen as carrier gas are used for detection of flammable products, in this case methane, ethane, propane and propylene. The operation principle is based on the detection of ions that occur during the combustion of organic compounds. The combustion takes place in a hydrogen flame, thus Hydrogen cannot be detected. Due to the combustion the FID is a destructive detector. The second detector used is a TCD. It is a universal detector which is based on detecting differences in thermal conductivity of a gas stream and compares it to the thermal conductivity of a reference gas, in this case Argon. The thermal conductivity is dependent on

the temperature and thus a parameter to adjust the TCD is the temperature of the detector. The TCD is set to 120 °C. Due to the separation of compounds in the columns the FID and TCD detects reaction gases one after the other and give a peak signal as output of the analysis. From the input the gas stream is directed to the first column which has a valve at the end and leads to the front FID (Front detector of the Gas Chromatograph detecting hydrocarbons (FID Front)). After 2 minutes the valve is switched and the gas that has not been flown through the column is redirected to the second column. The time is set in order to split $H_2$ and $CO$ from the main flow and send it to the second column. From there the gas flows through the TCD and then through the nickel catalyst and finally through the second FID labelled Back detector of the Gas Chromatograph detecting $CH_4$ after conversion form CO by a Nickel catalyst (FID Back) from now on. The nickel catalyst has the purpose of converting the reaction product $CO$ into $CH_4$ in order to be able to detect it with a FID detector. Although the TCD is an universal detector it is dependent on reasonable differences in thermal conductivity between the reference gas and the analyte. $CO$ has a thermal conductivity of 32,2 $mW/mK$ at 400K ([39]) and Argon of 22,6 $mW/mK$ ([40]) at 400K. For comparison, $H_2$ has thermal conductivity of 230,4 $mW/mK$ at 400K ([9]). Thus, the sensitivity of the TCD for $CO$ is rather low. For this reason the nickel catalyst is used. The column system is shown in the Figure below. The output signal of the GC is a chromatogram which shows the detector resonance on the x-axis and the time on the y-axis. The time corresponds to the retention time of the gas in the column system. A quantitative analysis is only possible if the peak areas can be referred to a reference. A pressure meter and a pressure regulator (manufacturer)are used for pressure control in the system. The pressure in the cell should be 1atm, the slightly higher pressure ensures that losses in the tubes are accounted for. An electric liquid pump (manufacturer) controls the flow speed of the gas in the tube system.

## 3.2 Experimental procedure and environment

The temperature of the cell and all chemicals is assumed to be constant 21.5 °C during all experiments (laboratory temperature). No cooling or heating was done. The cell was rinsed with water, flushed with nitrogen and rinsed with electrolyte prior to every experiment. During electrochemical reduction the pressure at the pressure regulator was kept constant at 1.08bars. The pressure meter showed after achieving steady state a pressure of 1.069 bars to 1.071 bars. After reaching steady state conditions in the cell, electrolysis is conducted and the reaction gas is captured in the gas loop. Thus, the gas is mixed with the $CO_2$ stream and circulates through the cell and the GC. At the end of the electrolysis, the product gas distributes evenly in the gas stream for 3 minutes. After that the GC is turned on and takes a sample of the gas. The valves of the tube systems are opened and the loop is flushed with $CO_2$ from the supply bottle for 5 minutes in order to remove product gases.

## 3.3 Cleaning

The importance of an impurity free environment during $CO_2$ reduction was explained in chapter 2.4.4. The cell has to be cleaned thoroughly before each experimental session. Therefore, all glass works (cells and beaker) were sonicated in a bath of concentrated H2SO4 for 8 hours in order to remove organic and metal contaminations (see chapter contaminations). Afterwards the cell is rinsed with MilliQ-water and boiled twice for at least 1 hour in MilliQ Water. Finally the cell is rinsed with electrolyte and flushed with nitrogen gas to dry.The electrodes

are submerged in concentrated $H_2SO4$ before the start of measurements in order to remove organic contamination and rinsed with MilliQ water and electrolyte solution. No mechanical or electrochemical treatment was done.

## 3.4 Gas chromatograph calibration

The GC was calibrated with a gas sample containing the gas concentrations displayed in table 3.1. The calibration set up was equal to the $CO_2$ reduction set up. The sample gas it flushed through the electrochemical cell and cycles through the tube system for 20 minutes. 5 different measurements were conducted. The final calibration method for the gas chromatograph was obtained by analysing step by step the sensitivity of the gases. GC parameters like flow rate, detector temperature and valve times were optimised. The main products of $CO_2$ reduction

| Compound | concentration |
|---|---|
| $CH_4$ | 0,102 |
| $C_2H_6$ | 0,152 |
| $C_2H_4$ | 0,203 |
| $C_3H_8$ | 0,152 |
| $C_3H_6$ | 0,098 |
| $CO$ | 0,1 |
| $H_2$ | 0,999 |

**Table 3.1:** Sample gas concentration for GC calibration

on a gold electrode are $CO$ and formate. For copper different other gases can be expected like methane, $CO$ and ethane. Hydrogen is a reaction product both on gold and on copper surfaces. It is detected in the TCD in the second Column. $CO$ is separated in the first column and is then captured by backflushing it towards the seconds column of the GC and towards the TCD, nickel catalyst and the FID. The nickel catalyst is working at 375 °C and converts $CO$ to $CH_4$ which is detected in a FID detector afterwards. All other gases go through the first column and are analysed in the FID Front.The calibration data and selectivity of the GC for the Front FID can be seen in the table below. The results from the calibration suggest a good sensitivity for all reaction products (see tables 2 and 1. The sensitivity is calculated by division of peak area with molar concentration of the sample gas. The FID Front shows high sensitivity for all gases. The TCD has a very low sensitivity for $CO$ what was expected due to similar thermal conductivity of $CO$ and the reference gas argon in the TCD. Methane that was converted from $CO$ in the nickel catalyst shows a better sensitivity in the FID Back, thus $CO$ can be analysed. The major products of $CO2$ reduction on a gold electrode are $CO$ and formate. For copper different other gases can be expected like methane and ethane. Hydrogen is a reaction product both on gold and on copper surfaces. It is detected in the TCD in the second Column. $CO$ is separated in the first column and is then captured by backflushing it towards the seconds column of the GC and towards the TCD, nickel catalyst and another FID (FID Back). The nickel catalyst converts $CO$ to $CH_4$ which is detected in a FID detector afterwards. All other gases go through the first column and are analysed in the FID Front. The calibration data and selectivity of the GC for the FID Front can be seen in table 1 and 2 in the appendices. The results from the calibration suggest a good sensitivity for all reaction products. The sensitivity

is calculated by division of peak area with the molar concentration of the sample gas. The FID Front shows high sensitivity for all gases. The TCD has a very low sensitivity for $CO$ what was expected due to similar thermal conductivity of $CO$ and the reference gas argon in the TCD. Methane that was converted from $CO$ in the nickel catalyst shows a better sensitivity in the FID Back, thus $CO$ can be analysed. The nickel catalyst was tested by using different concentrations of $CO$, i.e. 0.1 and 1 and comparing the results of the TCD with the FID Back. The catalyst works properly and converts the $CO$ into $CH_4$ completely. The sensitivities for $CO$ (TCD) and $CH_4$ (FID Back) are the same for both concentrations. This means that the peak areas show a linear behaviour against concentration which concludes with a well working catalyst.

### 3.4.1 Summary

The calibration of the gas chromatograph was successful. All expected reaction products can be detected by the set up. $CO$ shows low selectivity in the TCD but can be detected as $CH_4$ in the FID Back after conversion. The conversion is successful and complete and shows no deviation for a change of concentration. The tube system is leak tight and has only small dead volumes which have to be accounted for.

### 3.4.2 Volume Determination

A volume is considered to be an environment where the ideal gas law is valid. Then, the volume V can be calculated if the partial volume of all gases is known.

$$V = \sum_i V_i \tag{3.1}$$

The partial volume of the gases are calculated directly from the gas law:

$$V_i = (n_i \cdot R_g \cdot T)/(p_i) \tag{3.2}$$

with $R_g$ being the universal gas constant, $p_i$ the partial pressure of the gas and T the Temperature. The number of moles present in a gas mixture $n_i$ can be determined by applying a controlled reaction where the number of moles reacted is known. Such a reaction is the hydrogen Evolution reaction (HER) an aqueous acid solution.

$$2H^+(aq) + 2e^- ß H_2(g) \tag{3.3}$$

Hydrogen is created from H+ from water proteolysis and enhanced by a surplus of H+ in acid environment at the electrode surface. Two electrons are needed for the reaction. Thus the the number of substances can be calculated from Faraday's law.

$$n_i = Qi/(F \cot zi) \tag{3.4}$$

with Q being the electric charge associated to hydrogen generation, F being Faraday's constant and z the number of electrons needed for each hydrogen molecule. The gas will be captured in a closed system and disperse evenly in the volume. The molar fraction of a gas i in a gas mixture is defined by:

$$x_i = n_i/(n_{total} \tag{3.5}$$

If the molar fraction of gas i is known in the gas mixture, the total number of moles in the gas can be calculated by:

$$n_{total} = (n_i/(x_i) \tag{3.6}$$

and thus, the total Volume becomes

$$V_{total} = ((n_i/x_i) \cdot R_g \cdot T)/(p) \tag{3.7}$$

In Summary, the Volume can be calculated by applying the HER in a closed system and when Faraday's law and the ideal gas law are valid by

$$V = ((Qi \cdot R_g \cdot T)/(p_{total} \cdot F \cot zi) \cdot x_i) \tag{3.8}$$

As derived with 3.8 the volume of the tube system including the electrochemical cell can be determined electrochemically. In closed loop mode the gas cycles in a closed tube system. The Volume of the system can be determined electrochemically. A controlled reaction with a known number of generated molecules can be used for this purpose. The Hydrogen Evolution Reaction (HER) on a platinum electrode in acid aqueous solution is an appropriate reaction. The voltage region of hydrogen evolution is well known and hydrogen is the only gas being produced at the working electrode. While applying a potential between the electrodes, hydrogen is generated on the working electrode and oxygen on the Counter electrode. The product gas of the working electrode chamber is caught and directed to a chromatograph. The peak area resulting from the hydrogen generation is compared to the calibration data what gives the molar fraction of hydrogen in the gas mixture if the total pressure is equal to the pressure during calibration, i.e. 1,08 bar. In the calibration a peak area of 1768,97 was obtained for a molar fraction of Hydrogen of 1% at 1,08bars. During HER, if the total pressure is assumed to be fairly constant, the molar fraction of Hydrogen in the closed tube system can be determine by

$$molarfractionofhydrogen = ((peakAreaHydrogenduringHER)/(peakAreapermolfromcalibration)) \tag{3.9}$$

The charge Q is transferred from the working electrode to the counter electrode what is given by the potentiostat. This charge is associated to the HER. The charge refers to the number of hydrogen atoms reduced on the platinum electrode. 0.5 M sulphuric acid ($H_2SO_4$)is used as electrolyte in all chambers of the cell, i.e. as electrolyte in the reference electrode compartment, the working electrode compartment and the counter electrode compartment. Working electrode and counter electrode compartment are separated with a PE-Membrane. A $Hg/Hg_2So_4$ reference electrode is used and has a given potential against SCE of -0.682 V. The liquid volume of the working electrode chamber is 25 ml. The working electrode is a plane Pt electrode that was cleaned in sulphuric acid and rinsed with MilliQ water prior to the experiment.

**Method for Volume determination**

- 0,5min stabilization
- 2min reaction with several voltages applied
- 3min keeping the gas flow in a loop after reaction
- GC measurement to determine the hydrogen evolution in the cell
- 3min flushing with Argon
- 0,5min stabilization

Figure 3.4 shows the linear relationship between charge associated to hydrogen evolution and peak area from the TCD for the voltage as a parameter. The linearity is an indication for

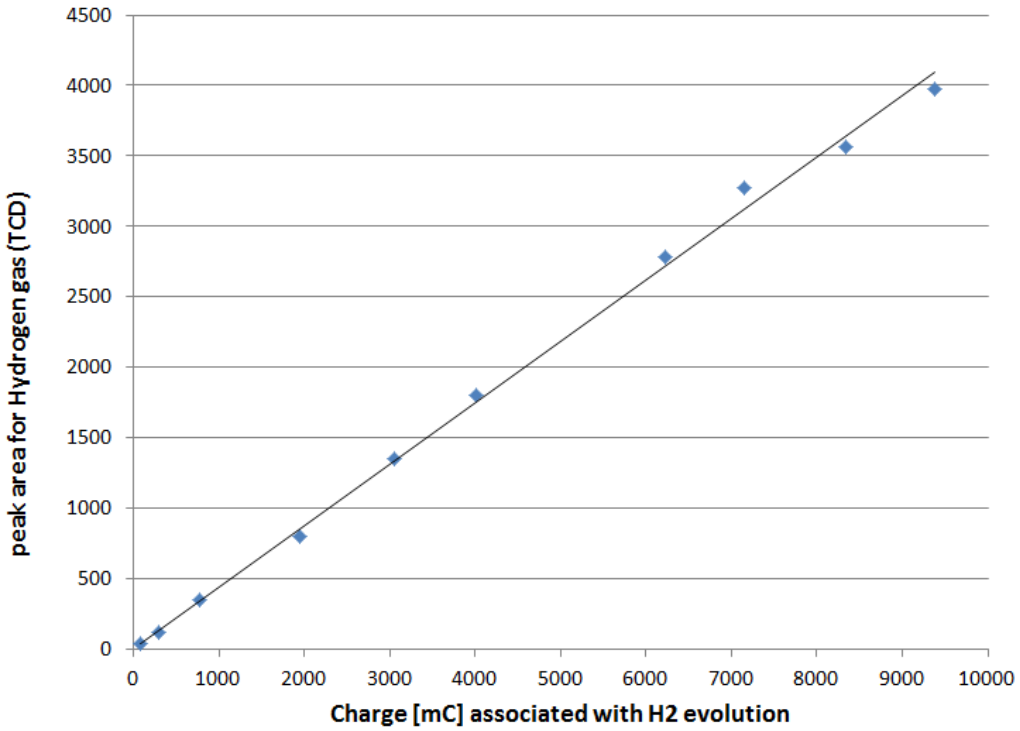


**Figure 3.4:** Results of Volume Determination. The graph shows that the results from the TCD for Hydrogen go well with the results from the charge transfer associated to hydrogen generation. Thus, the number of hydrogen molecules calculated from the charge and detected in the GC with the calibration data are equal.

| Potential (RHE) Volume[ml] | Potential (MSE) | Charge[mC] | $H_2$ signal | n | $H_2/ntot$ |
|---|---|---|---|---|---|
| -0.05 | -0.7 | 83.0587 | 40.008 | 0.00022 | 43.10 |
| -0.07 | -0.72 | 289.864 | 112.69 | 0.0006 | 53.40 |
| -0.09 | -0.74 | 774.952 | 342.08 | 0.0019 | 47.03 |
| -0.11 | -0.76 | 1946.38 | 796.38 | 0.0045 | 50.74 |
| -0.13 | -0.78 | 3053.61 | 1349.4 | 0.0076 | 46.98 |
| -0.15 | -0.8 | 4019.58 | 1797.63 | 0.0101 | 46.42 |
| -0.17 | -0.82 | 6221.47 | 2785.12 | 0.015 | 46.38 |
| -0.19 | -0.84 | 7151.34 | 3277.24 | 0.018 | 45.30 |
| -0.21 | -0.86 | 8337.98 | 3564.09 | 0.0201 | 48.57 |
| -0.23 | -0.88 | 9376.07 | 3973.42 | 0.0224 | 48.99 |

**Table 3.2:** Summary of results from Volume determination by hydrogen evolution.

the reliability of the data from the GC and the Potentiostat. Table 3.2 shows the summary of volume determination with the results of each potential step. The average volume from the is 47.56 $cm^3$ and the total cell volume with the 25 ml liquid electrolyte used for all experiments in this work is 72.56 $cm^3$.

### 3.4.3 IR-Drop correction in the set-up.

The sensitivity of the set up for IR-drop corrections were tested with a series of cyclic voltammetry measurements. As already mentioned in chapter 2.3 $R_u$ is mainly dependent on the distance between the reference electrode and the working electrode and as well on the conductivity of the electrolyte. The distance can only be reduced by placing the working electrode accordingly in the compartment. Two different concentrations of electrolyte solution are used in the experiments. 0.1M $KHCO_3$ and 0.5 M $KHCO_3$. From the theoretical point of view the conductivity of the latter is higher and will have a lower uncompensated voltage drop. In order to measure $R_u$ an appropriate method has to be chosen. With 0.1 $KHCO_3$ $R_u$ was about 60 Ohms and in 0.5 $KHCO_3$ it is 16 Ohms. Due to the change in electrode position no direct conclusion to a conductivity value of the electrolyte can be drawn (can be taken from literature for $KHCO_3$). The method was applied several times and shows stable values. A small change in electrode position in the compartment gives a change of $+-$ 10 Ohms in $R_u$. The expected current range is between 0 mA and 20 mA or expressed in uncompensated voltage drop, between 0 mV and 20 mV/ohm. The applied voltage needs to be as accurate as possible and for this reason for all $CO_2$ reduction experiments IR was measured in advance and added as an automatic correction in the potentiostat software.

**Electrolytes**
For the copper experiments 0.1 M $KHCO_3$ electrolyte was used. It was prepared from deionized MilliQ water and KOH granulate. The resulting KOH solution was saturated with $CO_2$ in a one-compartment cell and purified by pre-electrolyses for 4 hours at -3 V vs $Hg/HgSO_4$ resulting in a current of 27 mA. Pre-electrolysis was conducted in a one compartment cell with two gold meshes used as electrodes. The reference electrode is connected to the counter electrode. The electrodes have to be removed quickly out of the cell while still applying cathodic potential to the cathode in order to avoid re-dissolution of ions.

**Electrochemical Measurement Apparatus**
The measurements were conducted with a Potentiogalvanostat from Bio-Logic SAS (Bio-Logic SAS, model SP300). To reach higher Voltages the channel board was connected to a booster card (2 A/30 V). The $EC - Lab^T M$ software package was used for voltammetric and IR-Drop measurements.

## 3.5 Electrode preparations

### 3.5.1 Copper electrode

A copper piece (13 cm) was submerged in pure HCL for 10 minutes and rinsed with deionised water. Afterwards it was rinsed with electrolyte solution. An iron wire (99:99) was mounted on the copper with copper foil (99:99). Copper foil and metal conductor are not submerged in the electrolyte.

### 3.5.2 Gold electrodes

In this section the preparation of the gold electrodes is explained.

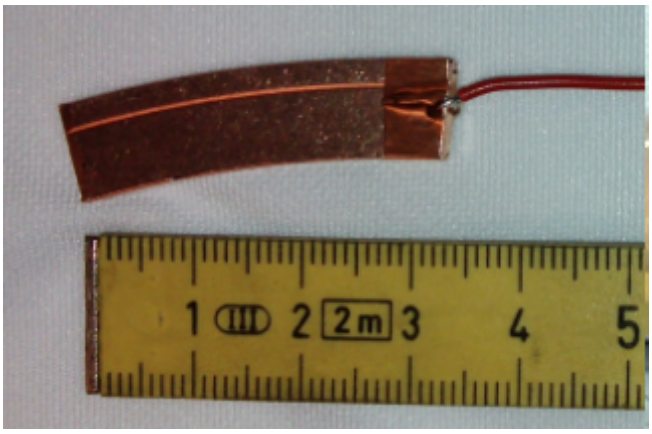


**Figure 3.5:** Copper electrode with iron wire mounted with copper foil

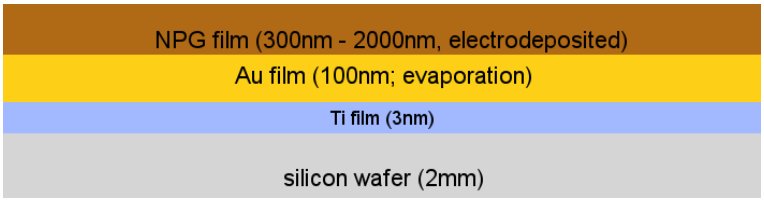


**Figure 3.6:** lateral $Cu$ of $Au$ electrode consisting of a silicon wafer as substrate, a 3nm $Ti$ film, a 100 nm $Au$ film form evaporation and a roughness factor dependent film thickness of NPG.

**Figure 3.7:** Schematic view of $Au$ electrode production

### Evaporation

The gold electrodes are fabricated with a 3" silicon wafer as substrate. On top of the wafer, a thin film of 3 nm $Ti$ and on top 100 nm $Au$ is evaporated in vacuum. On top of this layer a NPG film is electrodeposited (see Figure 3.7 The roughness factor of 1,1 was measured by $Cu$ UPD. An iron wire (99:99) with plastic cover was mounted on top of the $Au$ covered side of the wafer and retained with copper foil (99:99). The copper foil and iron wire were covered with resin in order to avoid contamination with $Cu$ or $Fe$ on the $Au$ surface. The resin was not submerged in the electrolyte. Further treatment is based on the described electrode.

### Electrodeposition

Different roughness factors of the gold electrodes were achieved by electrodeposition in the presence of $AuCl_3$. The real surface area was estimated by copper UPD, double layer capacitance measurements and oxygen reduction peak analysis. A summary of the deposition process is presented in TABLE 3.3. The electrodes are labelled according to the rounded roughness factors.

The procedure is explained in detail with electrode RF 6 now, for the other electrodes additional information can be found in the appendix. The measurements were conducted in the following order. First a CV with -0.6 V as the lower limit and +1.2 V vs $Hg/HgSO_4$ as the upper limit. The Voltage is cycled as a triangular wave between these values with a scan rate of 100 mV/s. To estimate the oxygen reduction peak area, followed by double layer estimation in the same cell. The electrochemical surface area prior to the deposition was analysed by copper underpotential deposition in a different cell. The formation of rough gold films was conducted in a third cell and finally $Cu$ UPD was done to determine the change in surface

| Electrode label | RF 1 | RF 2 | RF 6 | RF 10 | RF 15 | RF 17 |
|---|---|---|---|---|---|---|
| Projected surface Area [cm$^2$] | 1.5 | 1.5 | 1.5 | 1.5 | 1.5 | 1.5 |
| Roughness factor average [-] | 1.12 | 2.75 | 5.58 | 10.35 | 15.1 | 17.19 |
| Electrochemical surface area (ECSA) [cm$^2$] | 1.68 | 3.48 | 6.87 | 18.41 | 25.18 | 29.15 |
| ESA from UPD [cm$^2$] | 1.68 | 5.05 | 7.74 | 18.29 | | 27.17 |
| ESA from oxide reduction [cm$^2$] | reference | 3.48 | 7.5 | 18.41 | 25.18 | 29.15 |

**Table 3.3:** Summary of electrode preparation for $CO_2$ reduction.

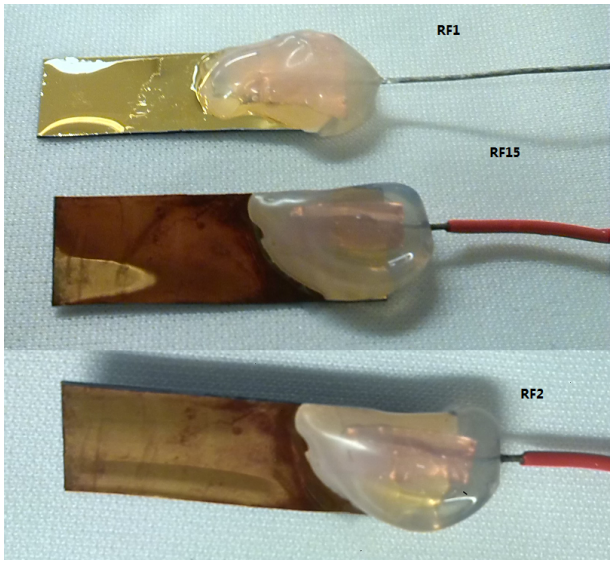


**Figure 3.8:** gold electrodes RF1, RF2 and RF15 with iron wire mounted with copper foil and a resin cover

area due to the deposition and in order to calculate the roughness factor. All measurements were conducted in 3 different one compartment prismatic cells with three electrode set up. A saturated $Hg/Hg_2SO_4$ reference electrode was used with a gold foil counter electrode and argon was flushed in all cells during 2 minutes before and during measurements. When changing cell the $Au$ sample was rinsed with MilliQ water and dried with nitrogen.

### Double layer capacitance and Oxygen reduction peak

The gold electrode was analysed with cyclic voltammetry in 100ml 0.5 M $H_2SO_4$ solution. For the reduction peak multi cyclic voltammetry measurements within -0.6 V to +1.2 V vs $Hg/Hg_2SO_4$ with 50 mV/s scan rate were conducted. The double layer region was determined to be within -0.1 V to +0.1 V vs $Hg/HgSO_4$ and cycled with 20 mV/s. The peak area (current vs. time) is integrated the get the charge associated to the process. For *RF6* the reduction peak area was 0.525 C.

### UPD before electrodeposition

Underpotential deposition with Copper ions was conducted in 120 ml 0.5 M $H_2SO_4$ with additional 1 mM $CuSO_4$. The potential was cycled between -0.460 V vs. and 0.1 V vs. $Hg/Hg_2SO_4$

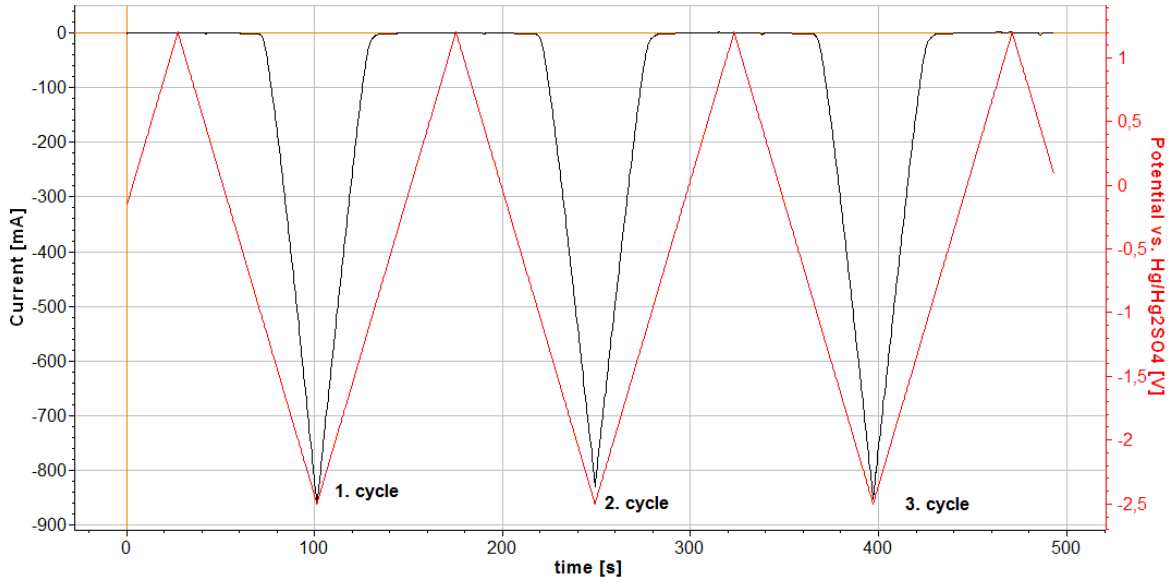


**Figure 3.9:** Waveform of Current and potential for electroplating. The linear potential ramp goes from +1.2 vs. $H_2SO_4$ to -2.5 V vs. $H_2SO_4$ for RF6. The red line represents the voltage, the black line the current.

with 20 mV/s. The potential was kept at the -0.46 V and 0.1 V for 45 s. This measurement was only done once for all $Au$ samples since it was assumed that the surface of the evaporated gold/silicon wafers have the same surface structure. For RF6, the charge associated to $Cu$ UPD was 0.707 C what gives an electrochemical surface area of 1.683 cm$^2$ and a roughness factor of 1.122 before deposition.

### Electrodeposition

Electrodeposition or electroplating was conducted with 100 ml aqueous 0.5 M $H_2SO_4$ electrolyte with additional 0.01 M $AuCl_3$ as gold source in a one compartment cell with three electrode set up. For the deposition process cyclic voltammetry technique was applied to control the cathodic and anodic region. In the cathodic potential region the deposition takes place. The voltage sweeps down with a scan rate of 100 mV/s to a low negative potential and cycles back to +1.2 V vs $Hg/Hg/SO_4$, the triangular wave form can been seen in Figure 3.9 where the current is plotted against time.. Depending on the Voltage, strong hydrogen evolution appears and the colour of the electrode changes from clear golden to brownish. In the anodic region an oxide layer is built up and reduced again at +0.55 V. After each cathodic sweep a change in the reduction peak is visible due to the increased surface area from the deposition process. It is the cathodic potential and the number of cathodic sweeps that determine the surface area and thus the roughness factor. By adjusting these parameters it is possible to control the deposition process. The figures 3.9 and 3.10 show the process for an electrode with RF17. Figure 3.9 shows the current as a function of time. For Rf17 the cathodic limit was -3.5 V and the increased current due to electroplating after each deposition cycle is visible. Figure 3.10 shows the current against applied Voltage vs. $Hg/Hg/SO_4$. The increasing oxide reduction peak area is visible after each cathodic sweep and a small shift of it to lower potentials as well. The $Au$ samples were cycled 3 to 5 times to the cathodic lower limits showed in Table 3.4 and +1.2 V: In literature more often pulse techniques are described for electrodeposition. The applied method here can be regarded as a very slow pulse technique. During measurements

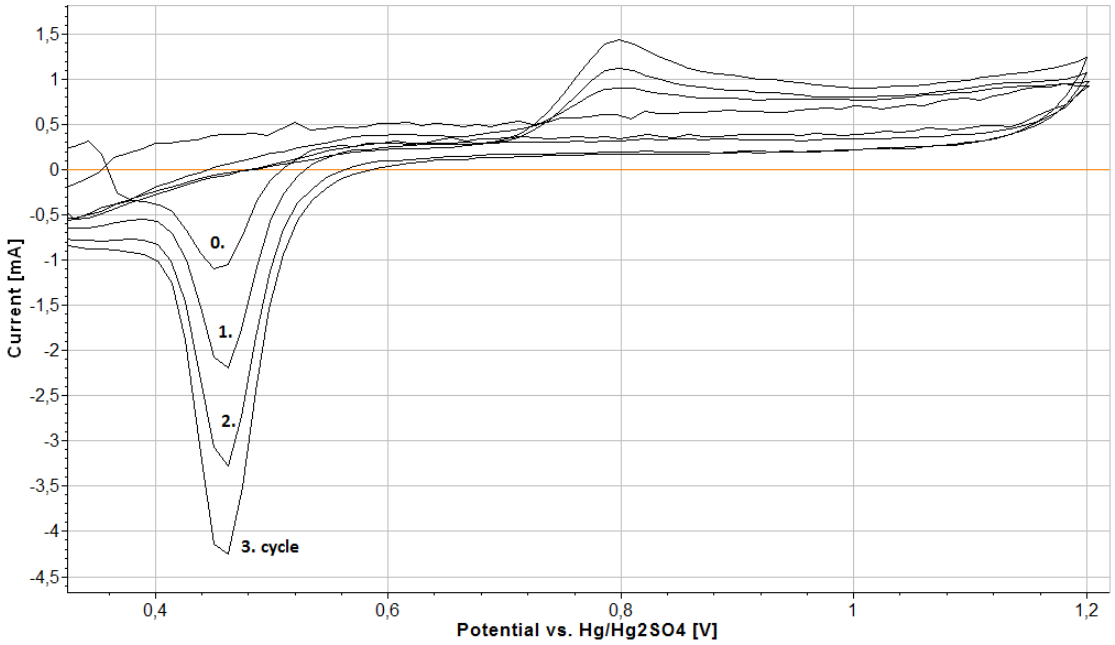


**Figure 3.10:** CV for electroplating process of RF6. The increasing oxide-reduction peak is visible at + 0.46 V vs. $H_2SO_4$.

| Electrode name | RF2 | RF6 | RF10 | RF15 | RF17 |
|---|---|---|---|---|---|
| lower cathodic limit vs. $H_2SO_4$ [V] | -2 | -2.5 | -3 | -3.5 | -4 |
| maximum current [mA] | -457 | 867 | 1060 | 1250 | 1460 |

**Table 3.4:** Lower cathodic limit and maximum current for electroplating procedure of the gold samples in 0.5 M $H_2SO_4$ and 0.001 M $AuCl_3$ . Upper anodic limit is +1.2 vs. $H_2SO_4$ and the scan rate is 100 mV/s

it was observed that the formed porous gold layer stripped off after a couple of cycles at high >-3.5V cathodic potentials and no change was observed anymore. An explanation could be that an alloying - dealloying equilibrium is established.

### Double layer capacitance and Oxygen reduction peak after deposition

The oxygen reduction peak after electroplating was analysed to compare it with the reduction peak before. It was conducted in the same cell and under the same conditions as before. As an example, the oxidation peak area for RF 6 changed to 2.773C which gives, divided by the value of 0.525 C prior to the deposition, a roughness factor of 5.717 after the deposition and thus an ECSA of 6.94 cm². Figure 3.11 shows the results for cyclic voltammetry before and after in 100 ml aqueous 0.5 M $H_2SO_4$ solution at 50 mV/s and flushed constantly with nitrogen. For the double layer region the results are contradictory. The double layer capacitance does not increase significantly so that this method was not taken into account for surface determination anymore.

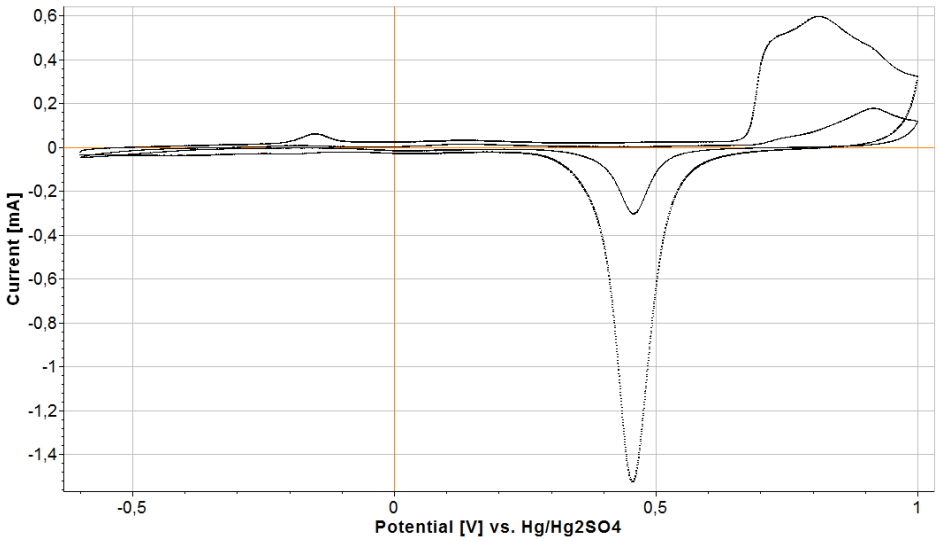


**Figure 3.11:** CV of gold sample before(sold line) and after (dashed line) the deposition. The roughness factor calculated from the oxide-deposition peak area is 5.71 $cm^2$.

### UPD after electrodeposition

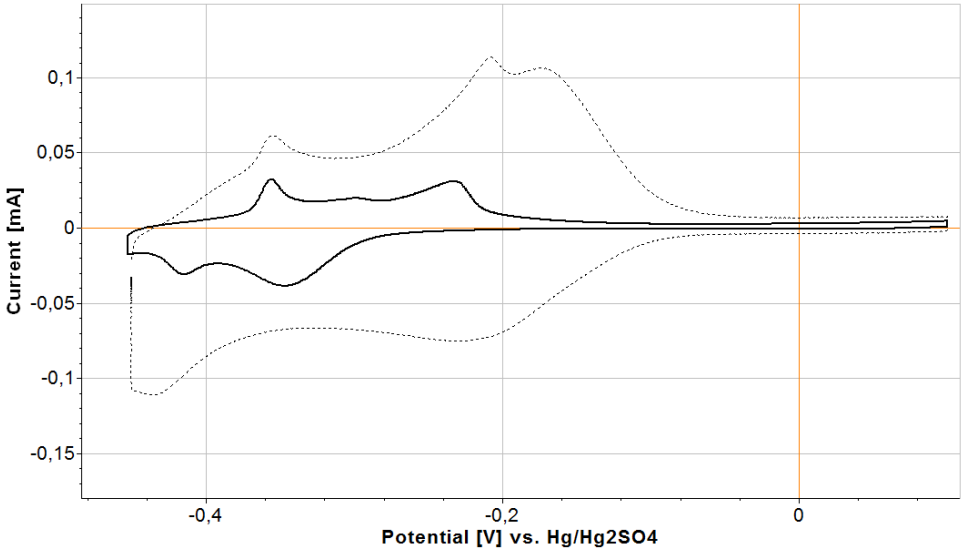


**Figure 3.12:** Results for Copper underpotential deposition for a gold sample (RF6) before (solid black line) and after (dashed black line) deposition. The graph shows the increase copper adsorption area due to an increased electrochemical surface area. The roughness factor calculated from the anodic peak area is 5.94 $cm^2$.

$Cu$ UPD after electrodeposition was conducted in the same cell as before and under the same conditions. The charge associated to $Cu$ increased to 3.251 C what gives a electrochemical surface area of 7.74 $cm^2$ and thus a roughness factor of 5.94. Figure 3.12 shows the results of $Cu$ UPD before and after the deposition. The solid black line refers to the state before the deposition and the dotted black line respectively to the state after deposition. Two peaks are visible in the anodic region as expected for Copper deposition. They refer to two different monolayer coverage rates of copper UPD on the gold surface. For Rf6 the averaged roughness factor is 5.86 what gives an electrochemical surface area of 6.87.

# 4

# Results and Discussion

## 4.1 Reproduction of Results with a plane copper electrode

A series of electrochemical reduction measurements were conducted with a plane copper piece with a projected surface area of 13.5 $cm^2$ . As electrolyte 0.1 M $KHCO_3$ was used at pH 6.8 measured prior to the experiment with a pH meter. The temperature was not measured nor controlled and is assumed to be room temperature, 21.5 °C, throughout the experiment. The IR-drop was measured with PEIS to be 29.4 ohms as can be seen in the Nyquist-diagram in Figure 4.1. The plot shows that there is inductance in the set-up which was not further studied. When plotting the frequency against the impedance of the electrolyte (Ru) and the double layer capacitance ($C_cl$) it is visible that the impedance goes against zero with increasing frequencies. The value for Ru increases to about 73 Ohms which is contradictory to the results from the PEIS measurement Figure 4.2. As a compensation for RU the value from the PEIS measurements was taken. The influence f the IR-Drop is rather small due to the small currents in the measurements what is the reason why this phenomena is not further studied here. Randle's circuit anyways

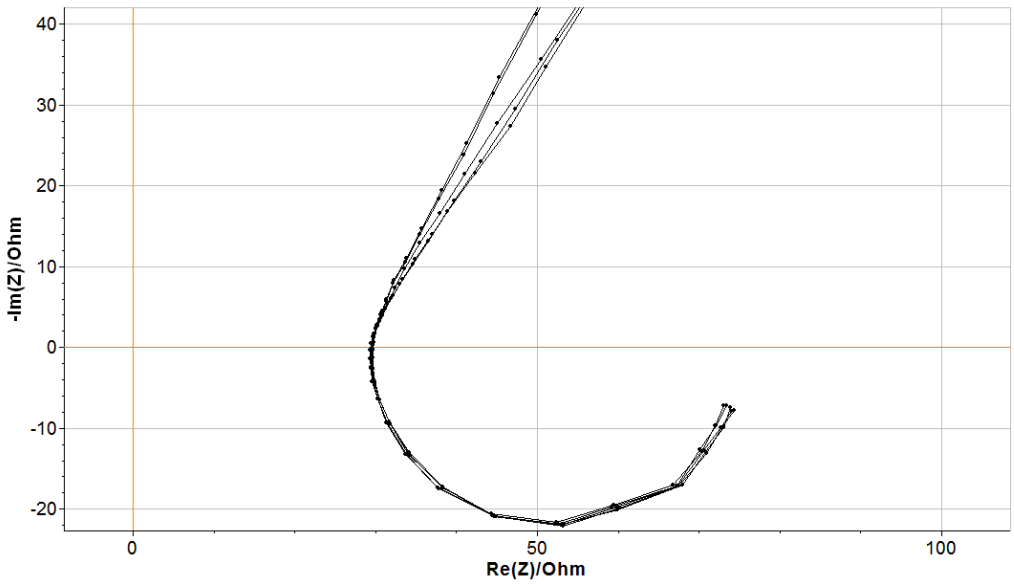


**Figure 4.1:** Nyquist diagram from PEIS of the electrochemical cell in three electrode set-up before electrolysis with copper electrode. Electrolyte resistance measured to be 29.9 ohms (left intersection with x-axis)

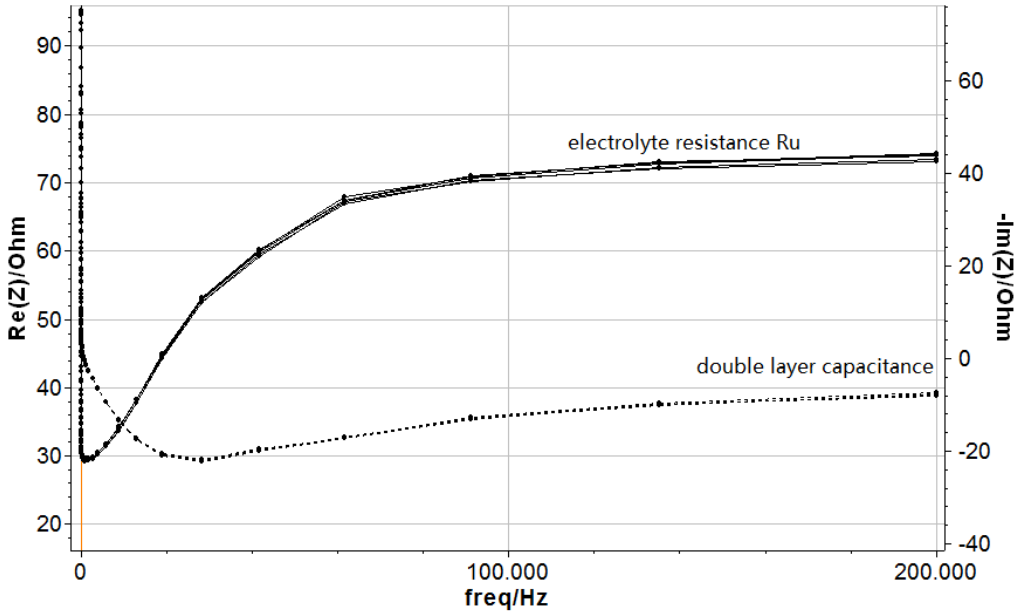


**Figure 4.2:** Electrolyte resistance and double layer capacitance plotted against frequencies measured with PEIS. Ru at 200000 Hz is 73 ohms

does not seem to be valid here in this case since inductance and contradictory results are visible from the frequency measurements. The voltage drop was accounted for automatically by the potentiostat software (EC-Lab V10.34) with 85%. Prior to the experiment a CV of copper was taken (Figure 4.3). The CV shows starting oxide formation at about +0.4 V vs. MSE. A small oxidation peak can be seen at -0.4 V vs. MSE which was not further studied but which might be an indication for impurities. All voltages presented from now are against Reversible

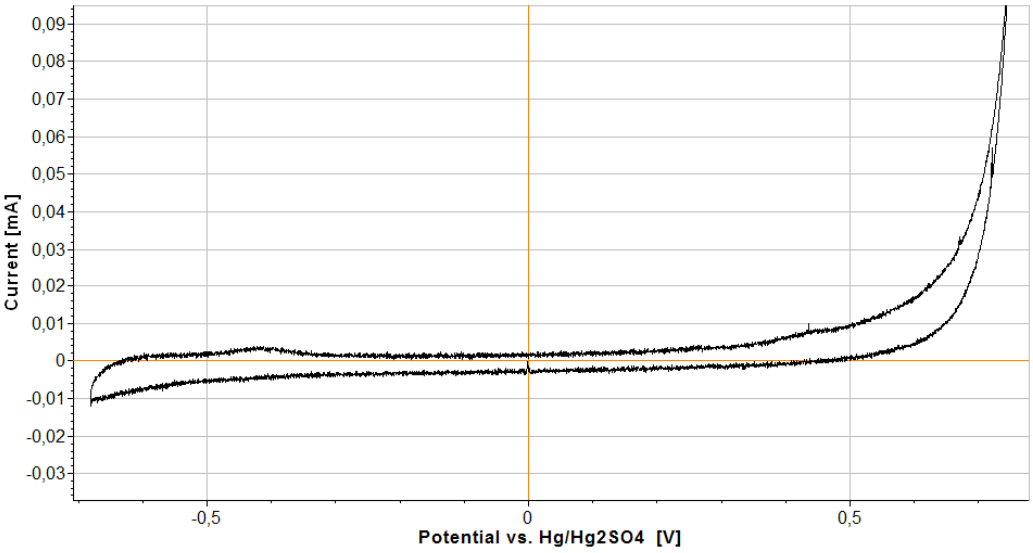


**Figure 4.3:** CV of copper electrode in 0.1 M $KHCO_3$ at 70 mV/s

Hydrogen electrode (RHE) if not stated otherwise. The measurements were conducted for 10 minutes between -0.558 V and -1.047V. The product distribution versus the voltage can be

seen in Figure 4.4. Hydrogen appeared to be the only product in the beginning of the series

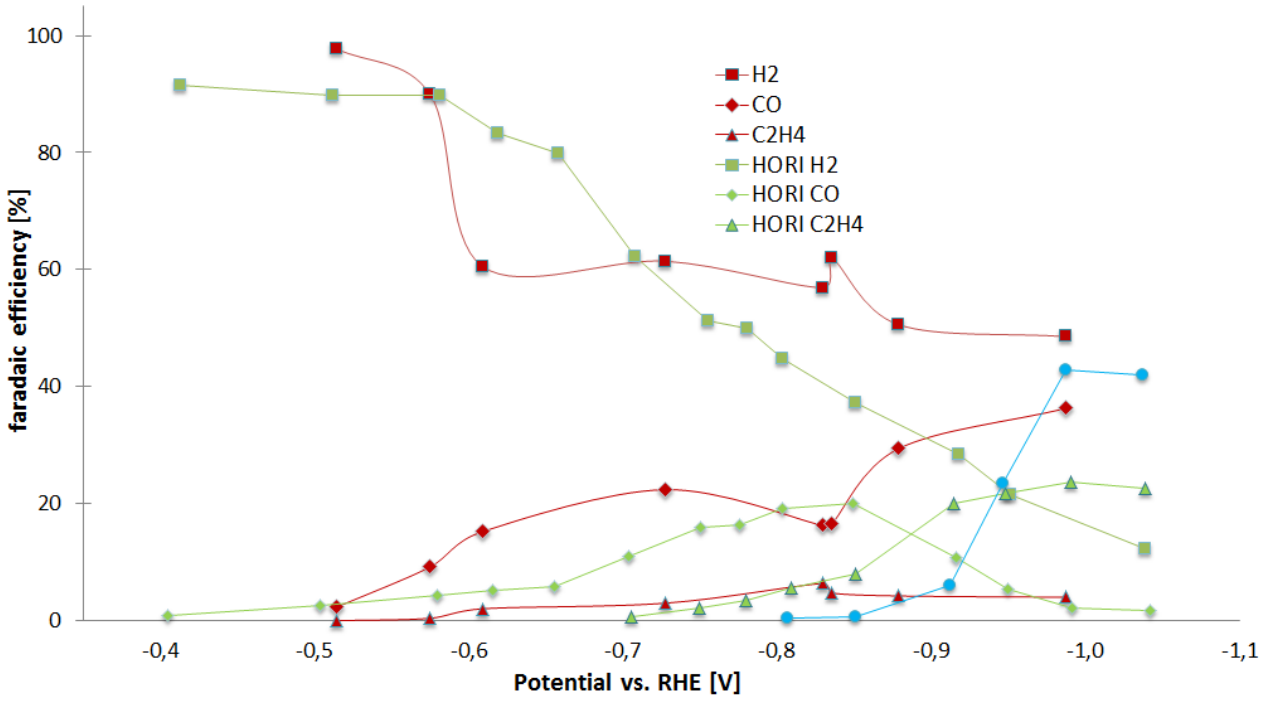


**Figure 4.4:** Gaseous products of $CO_2$ reduction for copper electrode in 0.1 M $KHCO_3$ plotted with literature results as presented in section 2.4.5

at -0.558V with 97.2 % faradaic yield. It drops down constantly to a minimum of 48.55 % at -1.047 V. *CO* appears the first time at -0.613 V with 9.18 %.and has a first peak at -0.728 V of 22.39 %. It then decreases slightly to 16.51% and ramps up again to the maximum of 36.29% at -1.047V. Ethylene stays almost constant throughout the series and never exceeds 6.5% faradaic yield. The total faradaic efficiency consisting of only gaseous products shows a drop from 97.2 % to 77.76 % between -0.613 V and 0.656 V and stays between 80 % and 90 %. The current density, see Figure 4.5, increases in the beginning from 0.4 mA/cm² to 1.2 mA/cm². After this peak at -0.728 V it drops again to 0.67 mA/cm² at -1.047V. The purpose of the experiment was to verify the experimental set-up and prove its capability to conduct electrochemical reduction experiments. This is done by comparing the results to Hori et. al. from 1989 which were already presented in section 2.4.5. There are few differences in the experiments that will be explained now. Hori conducts the experiments at 19 °C, thus a difference of 2.5 °C. The temperature dependence was presented in Chapter 2.4.4 and as a conclusion the difference can be neglected. Additionally Hori uses a electrodeposited copper sheet with a 8.5 cm² projected surface area in 60 cm³ electrolyte solution, compared to 13.5 cm² in 25 cm³. The electrode was treated mechanically and electrochemically prior to the experiment. No such treatment was done but cleaning the electrode in sulphuric acid and with MilliQ-water. *CO* shows a similar behaviour between -0.5 V and -0.9 V although the peak in Hori's experiments is at -0.85 V compared to -0.728 V with a slightly lower yield (22.39 % to 20.01 %). Whereas in Hori's experiments *CO* vanishes afterwards slowly as a product and methane and Ethylene production start, *CO* starts to increase after a small sink at -0.828 V. *CO* is assumed to be the key intermediate for hydrocarbon production. It appears to be also the limiting step that *CO* formation is the end of the pathway and no hydrogenation of *CO* occurs to form COH and hydrocarbons afterwards. The high yield for *CO* suggests that the *CO* molecule does not stay on the copper site after formation but strips off. This could

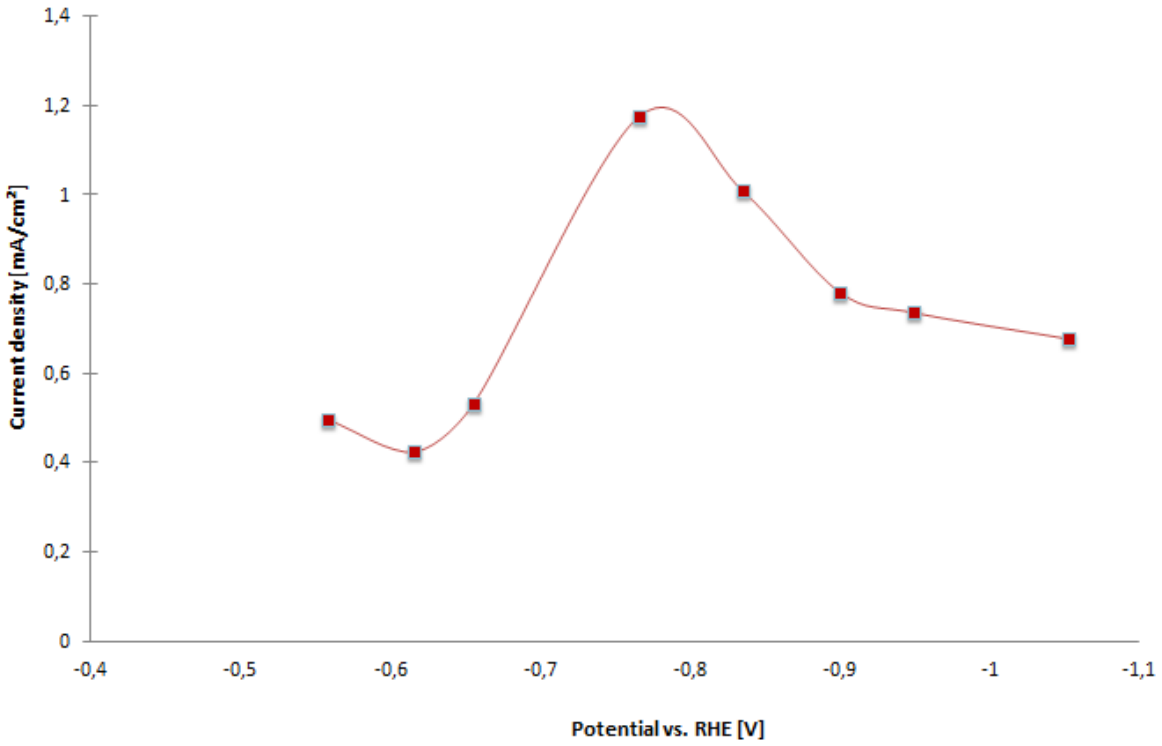


**Figure 4.5:** Current density of the copper electrode during $CO_2$ reduction.

be explained by very high convection due to $CO_2$ bubbling in the cell or hydrogen gas that pushes the $CO$ molecules from the surface. Hydrogen generation decreases rapidly from 89 % to 66.5 % between-0.613 V and -0.656 V respectively. After that it remains almost constant although it is expected to vanish. This could be explained by the change of surface morphology of the copper electrode. After the experiments the surface was covered with a black film which is described in literature as carbon deposition (Figure 4.6). The carbon is deposited on the copper sites and deactivates them. Carbon forms mainly hydrogen as a reduction product and thus the higher yield of hydrogen can be explained by carbon activity although the increase in $CO$ proves that carbon does not cover all copper sites. Hydrogen evolution could also be a

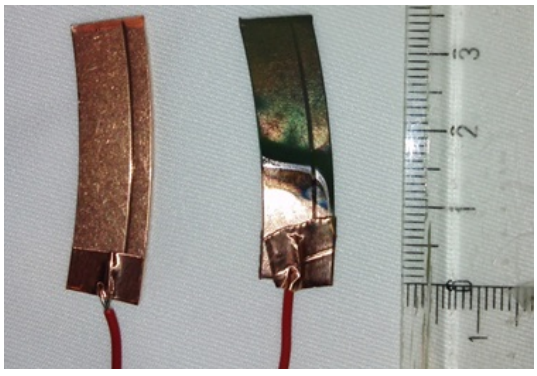

**Figure 4.6:** Picture of the copper electrode samples. Carbon deposition is visible after $CO_2$ reduction (right-hand electrode)

reason for the diminished hydrocarbon formation. Hydrogen gas formed on the surface might interfere with the loosely bound $CO$ molecule on the copper sites. The appearance of ethylene is remarkable in this context, since the C double bond seems to be formed rather than the simpler

molecule $CH_4$ although the faradaic yield is rather low. Reactions that can be accounted to $CO_2$ reduction make 38.29 % ($CO$ and $C_2H_4$) at -1.047 vs. RHE whereas 64.69 % ($CH_4$+$C2_{H4}$) can be accounted at -1.03 V vs. RHE in Hori's experiments. Regarding the development of the current densities a decrease can be observed at higher overpotentials which is contrary to Hori's results. Generation of hydrocarbons requires more electrons per molecule thus the lower current can be explained by little hydrocarbon formation. In summary the experimental set-up could be tested and verified. Differences with Hori's results might come from carbon contamination in the cell since the electrode was not electrochemically polished before the experiment. On the other hand carbon should be oxidized by treatment with sulphuric acid. The sum of the faradaic efficiencies match with the results of the gas chromatograph thus the calibration was successfully done. The set-up is leak tight since neither oxygen nor nitrogen were measured in the GC during the experimental series.

## 4.2 $CO_2$ reduction of gold electrodes

### 4.2.1 RF 1.12

A gold electrode was produced by evaporating gold particles on a silicon wafer. The gold film has a roughness factor of 1.1 and the surface in contact with electrolyte was about 1.5 cm² giving an electrochemical surface area of 1.68 cm². The electrolyte was 0.1 M $KHCO_3$ (pH 6.82). Several measurement series were conducted with different $Au$ samples (RF1.12) from which two are presented here. Prior to the experiment the IR-drop of the cell was determined with PEIS to be 63.1 ohm. Results from cyclic voltammetry before the start of the electrolysis do not indicate impurities or malfunctions of the electrode (Figure 4.7).

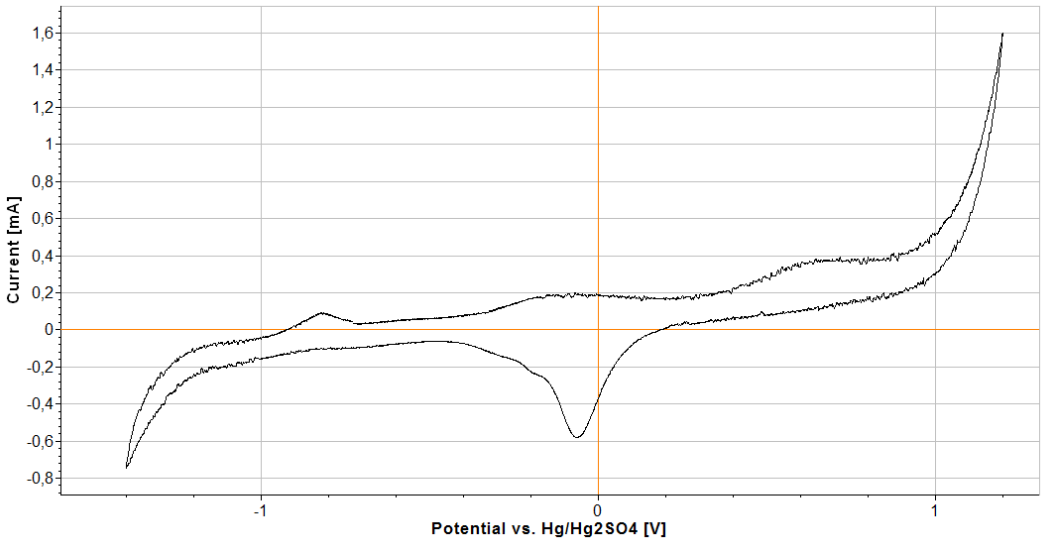


**Figure 4.7:** CV of plane gold electrode (RF1.12) in 0.1 M $KHCO_3$

Electrolysis was conducted in a voltage range between -0.436 V vs. RHE and -0.722 V vs. RHE with potential steps of 0.1 V for 10 minutes. The results are shown in Figure 4.8. $CO$ is between 50 % and 70 % FE throughout the experimental series. $H_2$ does not appear before -0.533 V vs. RHE but decreases slighty from 40 % FE to 24.66 %. The current density at -0.436 V is very low with 0.147 mA/cm². The GC shows sensitivity problems at such low gas concentrations. In the chromatogram a small peak is visible but not analysed what suggests

that hydrogen is a reaction product. In general the results are in good agreement with Kanan et. al. [41] for polycrystalline Au.

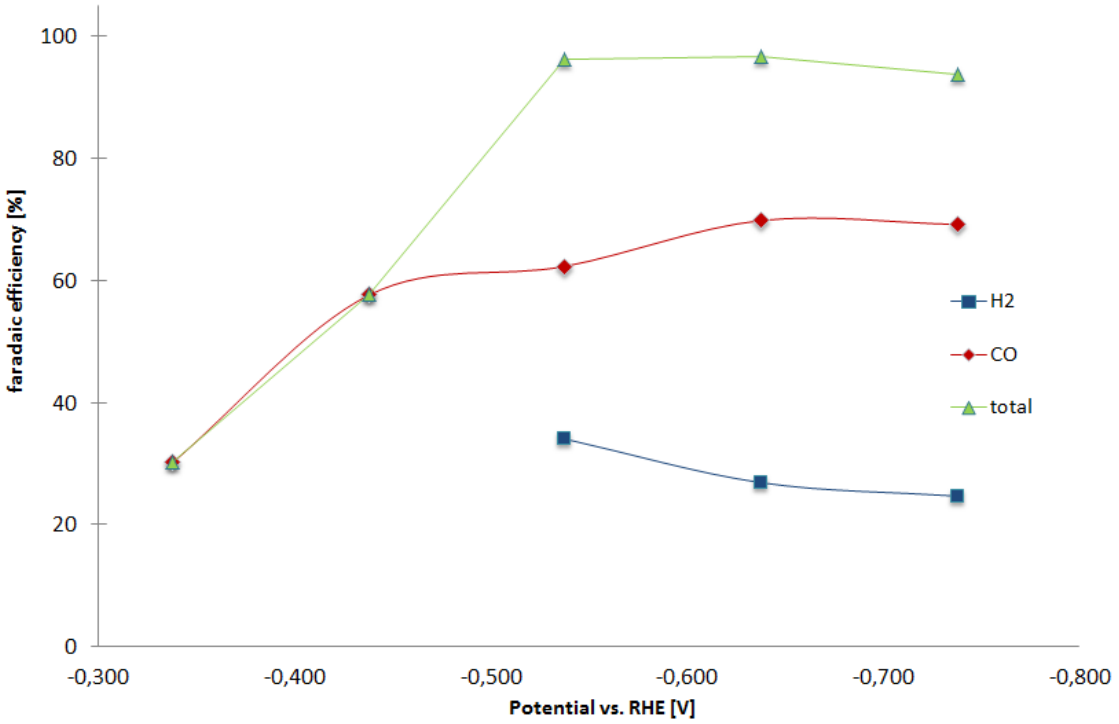


**Figure 4.8:** Gaseous products of $CO_2$ reduction for RF1(1) in 0.1 M $KHCO_3$

A second $Au$ sample with RF 1.4 and about 2.1 cm$^2$ surface area was used for electrolysis in order to see hydrogen production at lower potentials and for confirmation of the first results. The results were showed a deactivation from the beginning of the experimental series. The trend is similar though, since, but a shift to higher overpotentials is visible. Hydrogen appeared this time at lower potentials due to a longer reaction time.

### 4.2.2 RF 6

The gold electrode has a roughness factor of 5.71 and an electrochemical surface area of 6.87cm$^2$. The ohmic resistance $R_u$ was measured to be 53.4 ohms. The CV (4.10 shows a peak at -0.1 V vs. RHE which origin cannot be identified. The results can been seen in Figure 4.11. $CO$ formation starts already at a potential of -0.29 V vs. RHE with a faradaic efficiency of 7 %. In comparison to Kanan's group, that had a FE of about 10 % at -0.2V vs. RHE and a gold electrode with RF 72. At -0.336 V $CO$ increases to 33.49 % and hydrogen drops from 91.362 % to 65.153 %. At higher cathodic potentials the faradaic yield of $CO$ drops first to 6.51% and then increases slightly up uo 19.92 % at -0.624 V again so that their is a peak of $CO$ at -0.336 V. Repetition of this voltage point suggests deactivation of the gold electrode. Hydrogen shows a similar behaviour. The peak at -0.336 V is visible and the total efficiencies some up to 95 % to 98 % throughout the experiment. Compared to RF1 the FE is on the same level for -0.336 V. (33.49 to 31 %) but with a slightly higher current for RF6 what is expected due to the higher surface area. The difference in current though, does not represent a factor of 6, thus the current density is slightly lower. In order to analyse the reason for the deactivation of the gold electrode a XPS measurements were done with 3 different electrodes. One new $Au$ sample with RF 1,RF (Au1), RF6 (results just presented) and RF17 (not used for electrolysis)

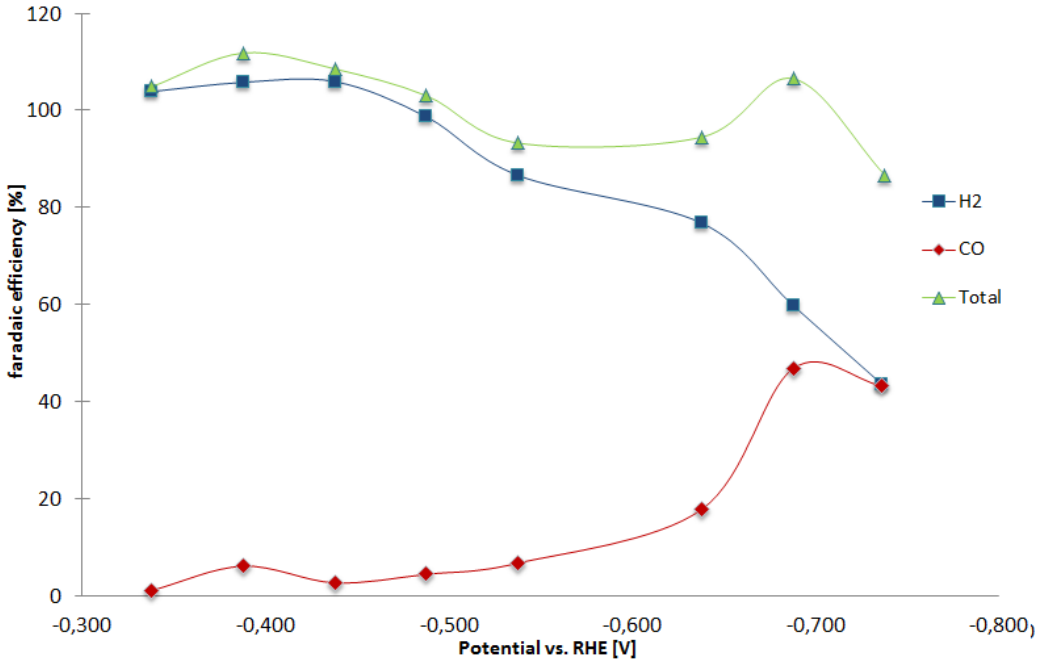


**Figure 4.9:** Gaseous products of $CO_2$ reduction for RF1(2) in 0.1 M $KHCO_3$

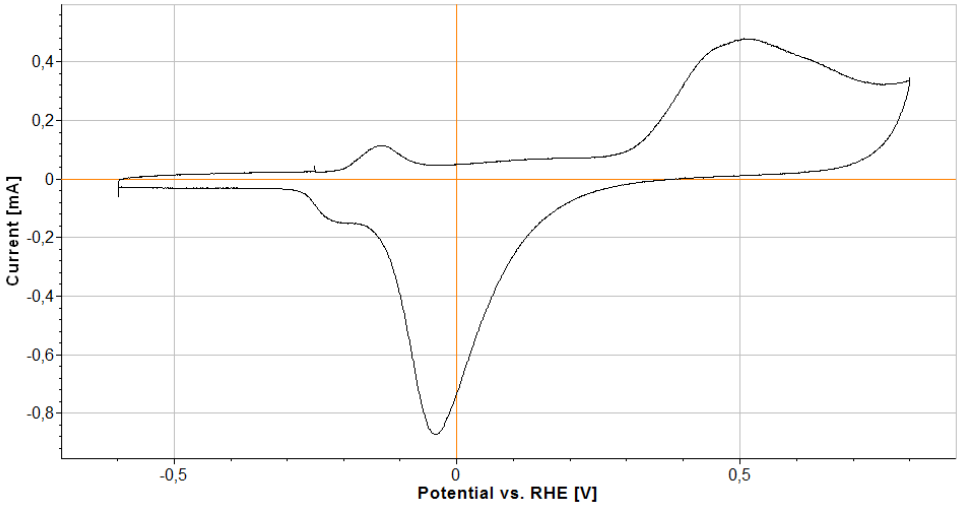


**Figure 4.10:** CV of RF6 in 0.1M $KHCO_3$

for comparison. The samples were rinsed with MilliQ water, dried and cut before the analysis. The photo-electron peaks associated to gold are listed in table 4.1 and the XPS results are shown in figure 4.12 For Au1 the peaks correspond clearly to gold. .

| electron config. | $5p_{3/2}$ | $5f_{1/2}$ | $4f_{7/2}$ | $4f_{5/2}$ | $5s$ | $4d_{5/2}$ | $4d_{3/2}$ | $4p_{3/2}$ | $4p_{1/2}$ | $4s$ |
|---|---|---|---|---|---|---|---|---|---|---|
| Binding ener.[eV] | 57 | 74 | 84 | 88 | 110 | 335 | 353 | 547 | 643 | 763 |

**Table 4.1:** Binding energies for $Au$ for characterisation in XPS

Additionally carbon and oxygen are visible. Carbon deposition on the surface might come from air, since the electrodes were prepared on air. For RF17, which was not used for $CO_2$

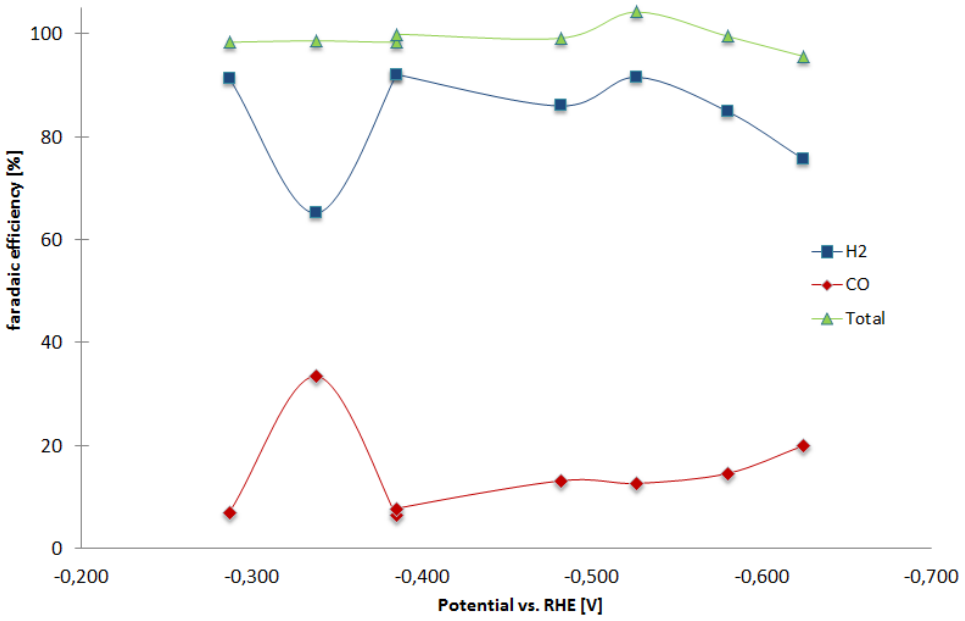


**Figure 4.11:** Gaseous products of $CO_2$ reduction for RF6 in 0.1M $KHCO_3$

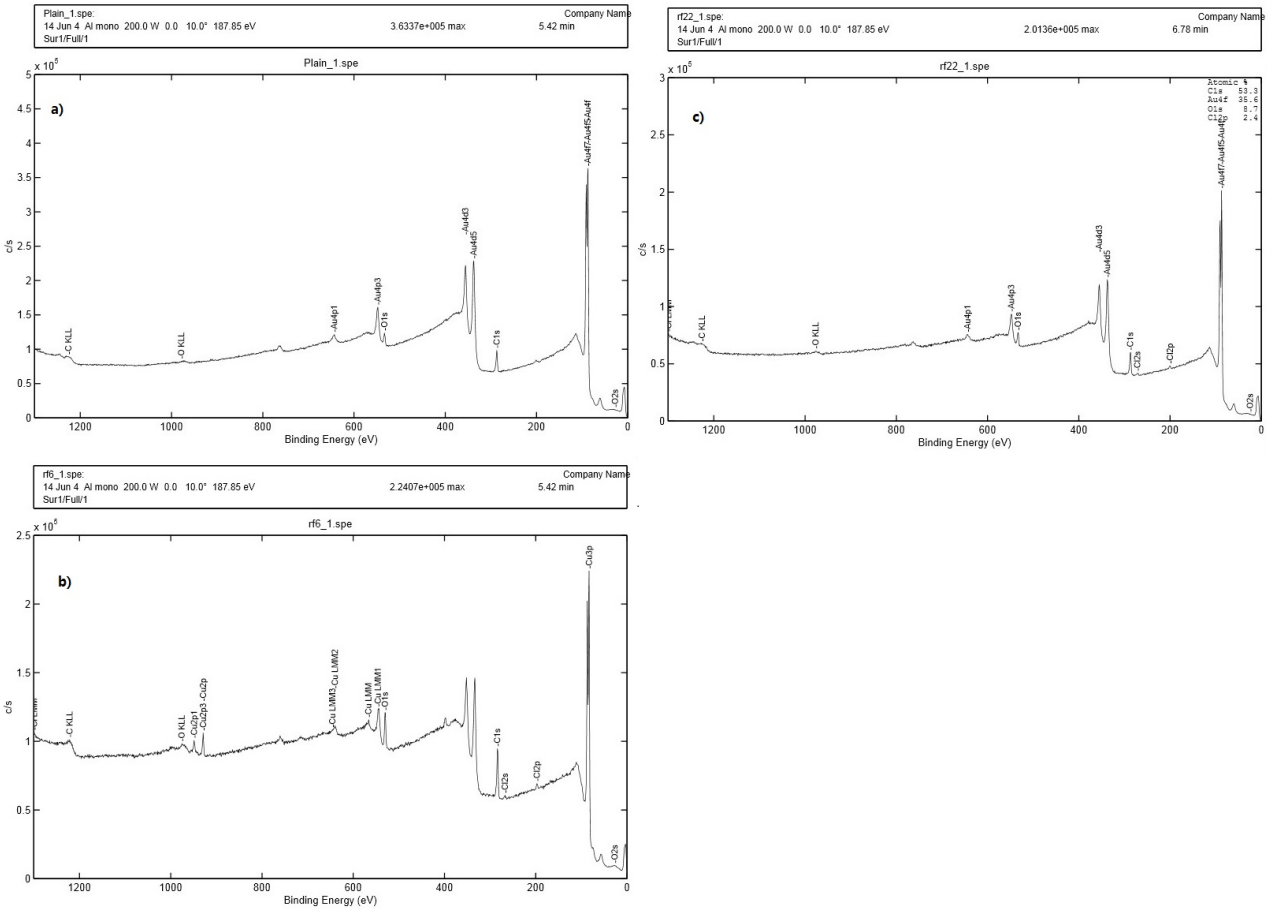


**Figure 4.12:** Results for XPS for the electrodes RF1, RF6 and RF22

electrolysis yet, the peaks also correspond mainly to gold. Similar peaks for oxygen and carbon can be seen but additionally a small peak for chlorine at 200 eV and 270 eV is visible. Rf6 shows

several differences compared to the other electrodes. The peaks at 932 eV and 951 eV can be associated to $Cu$ electrons ( $Cu2p_3/2$ and $Cu2p_1/2$). This is surprising since there is no copper source when conducting $CO_2$ electrolysis but the $Cu$ foil mounting the metal conductor. But this foil is covered by resin and not submerged in the electrolyte. Additionally the carbon peak at 287 eV is larger than on the other electrode. A monolayer coverage of carbon would be enough to deactivate $CO_2$ reduction selectivity of the electrode and enhance hydrogen evolution, since carbon forms mainly hydrogen as a reduction product. The appearance of the electrode after electrolysis did not change significantly. The rough NPG film has a darker colour similar to the blackening of the copper electrode used for verification of the set-up, thus carbon deposition cannot be detected visually.

### 4.2.3 RF 10

Based on the findings from Rf1 and Rf6 the electrode was only submerged into $H_2SO_4$ for 1 minute. Secondly it was electropolished by pulse voltammetry in 0.5 H2SO4. The current was set up to 2500 mA at a voltage of +30 V against Hg/HgSO4 and the pulse duration was about one second. The electrode was then thoroughly rinse with MilliQ water and electrolyte solution and dipped into the electrochemical cell with a potential kept anodic before contact with the electrolyte. The ohmic drop was measured at -0.6 V against $Hg/Hg_2SO_4$ to be 51.4 ohms and it is again corrected automatically. The counter electrode was regenerated in 0.05 M $H_2SO_4$ prior to the electrolysis for 10 cycles between 0.4 V and 1.4 V vs. $Hg/Hg_2SO_4$ at a scan speed of 100 mV. The treatment was stopped after the CV shape did not change anymore. After

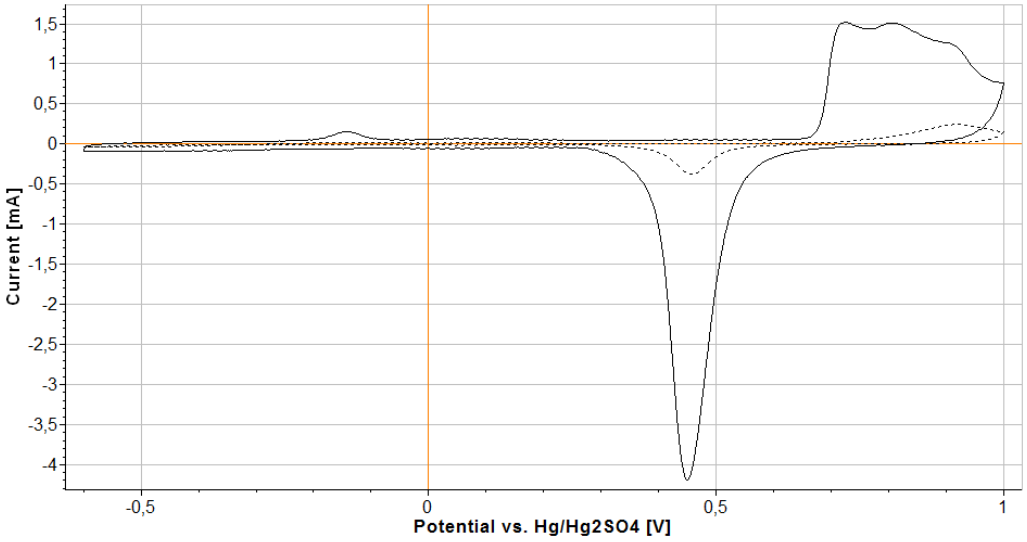


**Figure 4.13:** Comparison of CV before and after electroplating of electrode RF10 in 0.5M $H_2SO_4$. Increase of oxygen reduction peak is visible.

each reduction point the electrode was polarized with an anodic potential. The voltage was kept slightly anodic at -0.4 V vs $Hg/Hg_SO_4$ and a peak with a current of 0.4 mA appeared right in the beginning. The potential was kept for one minute and then returned to OCV. At a potential of -1.35 V vs. $Hg/Hg_SO_4$ the current remained constant on 0.323 mA. Another observation compared to RF6 is that the current was about 3 times higher than at RF6. The faradaic yield at this potential was 3,3 % for $CO$ and 89 % for $H_2$ and thus worse than for Rf6 with 7 %. Afterwards the Faradaic efficiency increased constantly to a maximum of 81.36 %

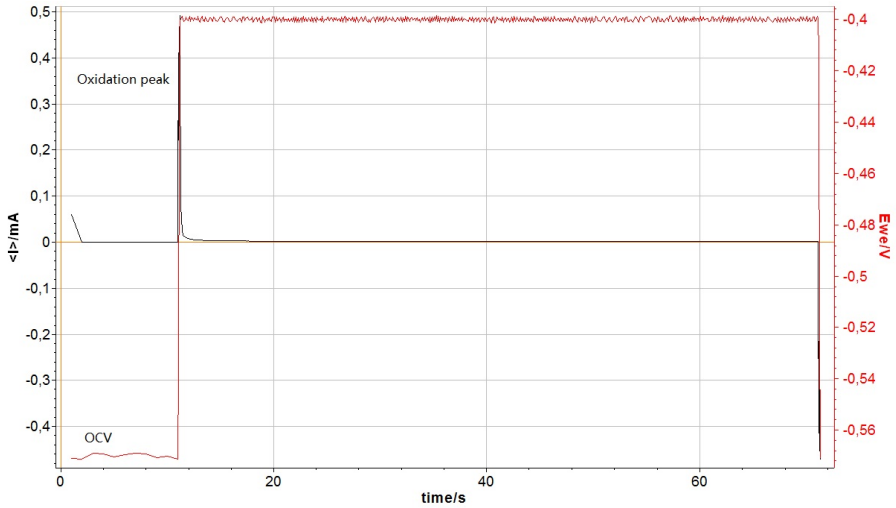


**Figure 4.14:** Anodic polarization after 20 min electrochemical reduction of $CO_2$. Potential was kept slightly anodic for 1 minute. Oxidation peak is visible.

at -0.467 vs Reversible hydrogen electrode (RHE). A summary of all roughness factors and a comparison to Kanan's results are given in the figure below.

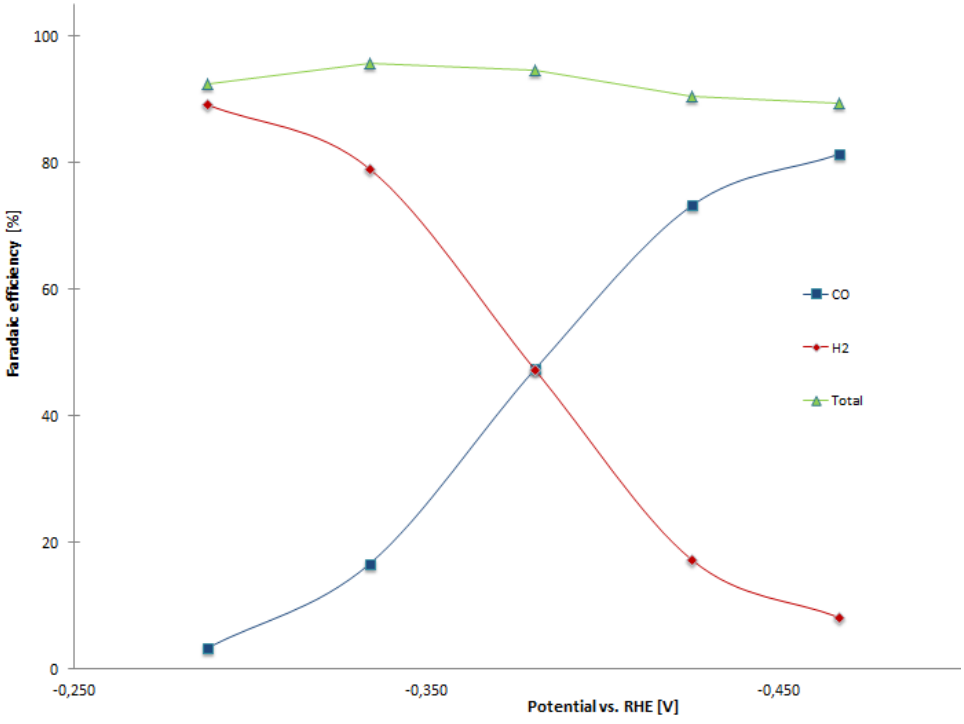


**Figure 4.15:** Results of $CO_2$ reduction for RF10 illustrated as faradaic efficency against potential vs RHE.

### 4.2.4 RF15

Current densities. the density should be much higher, more or less time RF?! This does not happen due to several problems with the porosity of the electrode. It can be assumed that the

mass transport in the porous plane is rather slow compared to a plane electrode. This might affect the pH of electrolyte within the porous layers. Secondly an accumulation of hydrogen gas might block parts of the porous layer.

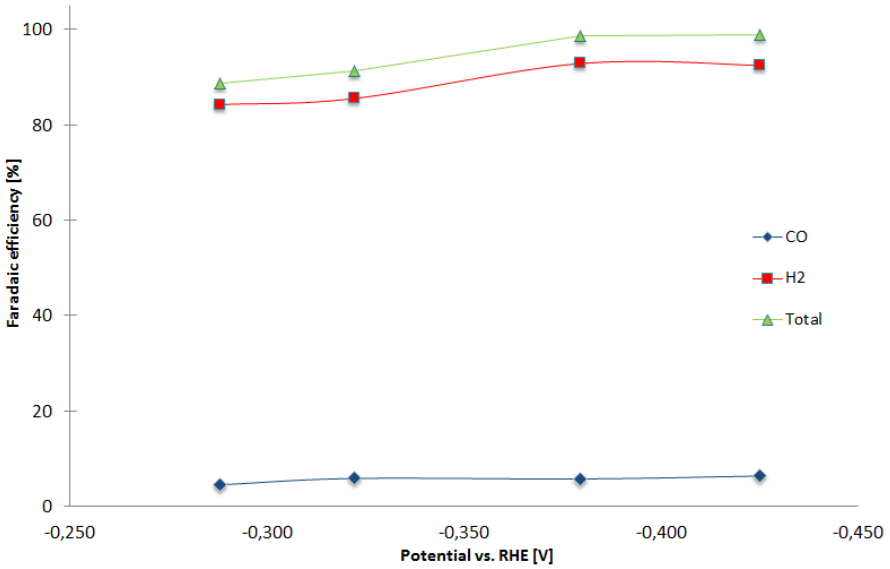


**Figure 4.16:** Faradaic efficiencies of $CO_2$ reduction plotted against potential vs. RHE for RF 15.

## 4.3 Analysis of Nanoporous gold film samples

Gold electrodes of different roughness were produced by electron beam evaporation and electroplating of $Au$ in an acidic solution. The different roughness factors were determined by $Cu$ UPD and the change of surface morphology is optically visible since the rougher electrodes have a darker surface. The surface structure was analysed by SEM (Scanning electron microscope) after electrochemical reduction of $CO_2$. The SEM images show the cross-sectional area of the electrodes. The darker parts in the bottom of the pictures show the silicon substrate. Figure

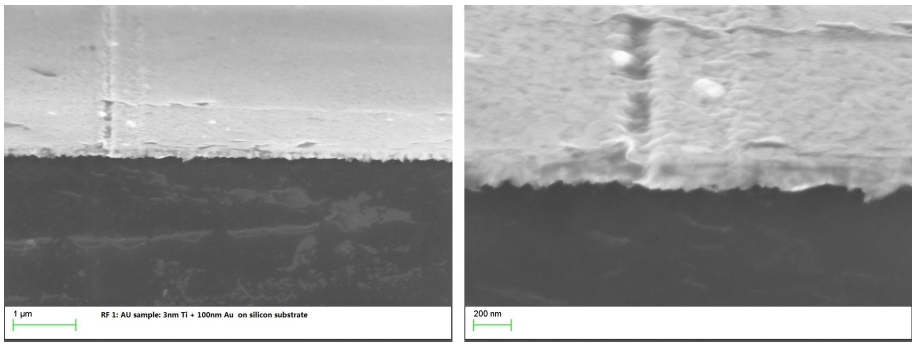


**Figure 4.17:** Cross-sectional SEM Image of $Au$ sample (RF1) with 3nmTi + 100nm $Au$ beam evaporated on a silicon substrate. ECSA is 1,56 and the Roughness factor is 1,02.

4.17 shows a SEM Image for the beam evaporated gold sample which is used as a base for electroplating. The results for electrochemical reduction were presented as RF1 with two different electrode samples in the chapter before. The SEM picture refers to RF1 (1) and indicates that

the evaporated film is about 150 nm thick; however the tilted view may alter the dimensions. The surface is rather flat and no particles are distinctive on top. The SEM image also shows that the film is not porous and the structure is packed. The line of breakage between the silicon substrate and the gold film is uneven due to rather uncontrolled cracking of the electrode. In general the surface looks rougher than the results from *CO* UPD indicated but a change in current density before and after electrochemical reduction was not observed. Figure 4.18

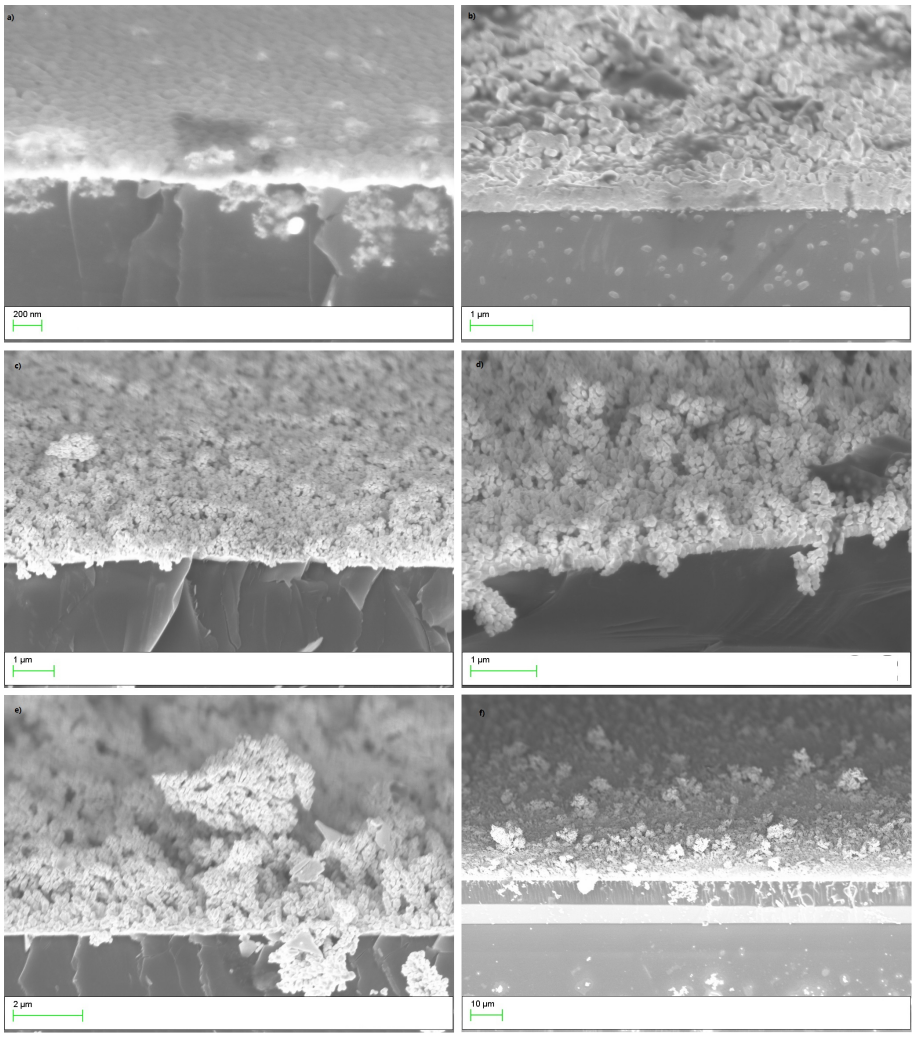


**Figure 4.18:** Cross-sectional SEM Images of nanoporous *Au* samples (a: RF2; b:RF6; c:RF10; d:RF15 e:RF17; f:RF 17) with 3nm Ti + 100 nm *Au* beam evaporated on a silicon substrate and electroplating of *Au* particles on top

shows SEM Images of all nanoporous *Au* samples prepared as presented in the chapter before. The labelling refers to the same electrodes. The SEM images show that the film thickness increases from about 200 nm for Rf2 to about 2 $\mu$m for RF17 including the evaporated gold film. The particle size does not change for different roughness and the particles have an oval shape. The length is about 200-250 nm and the width is about 150-180 nm. No statistical analysis of the particle size was done. *Au* sample RF2 has a rather symmetric surface structure. No clusters on top of the film are visible and the particles are packed next to each other in a dense formation. The rougher electrodes have an unstructured surface and gold particles agglomerate in different cluster sizes on top. The size of the clusters seems to increase with increasing roughness factor. Figure 4.18 f shows the surface morphology of *Au* sample RF17 and gives an indication for the upper limit of the roughness factor for the applied electroplating

method. Big clusters of 1 - 2 $\mu$m size built on top of the film. The $Au$ particles found after electroplating could be these stripped off $Au$ clusters. Kanan at al. produced nanoporous $Au$ samples with a similar film thickness but much lower particle size of about 20 - 40 nm. The group concluded that the particle size is not the dominant factor, since SEM images after 8h electrolysis indicated a sintering of the surface accompanied with increasing particle and cluster size. The RF dropped from 72 to 17 without reducing the selectivity of $CO$ reduction but with reducing the current density. No SEM pictures of the sintered surface were shown so that a comparison is not possible, however RF17 was not used for electrolysis and the surface does not appear to be sintered or altered compared to the other electrodes although the roughness factor was determined electrochemically prior to SEM.

## 4.4 Set-Up

The set-up was verified to be able to conduct experiments with electrochemical reduction of $CO_2$ on different electrodes. The gas system is leak tight and the analysis with a gas chromatograph works properly. The flow rate of the $CO_2$ flushing can only be adapted through the regulator of the electric pump. A flow meter that was installed was seen to be the reason for leakage and was removed. The regulator of the pump can only be adjusted by the percentage of engine power of the pump, thus no quantitative value of the flow speed is possible. The flow speed though, has an influence on the current density of the electrode. If, during a reduction experiment, the pump speed is decreased slightly, a drop in current is visible in the potentiostat. The flow speed has an influence on the mass flow in the electrolyte. The electrolyte is installed in the cell manually. The position towards the reference electrode and also towards the $CO_2$ gas outlet is changed slightly for every experiment. The pump speed was set manually and the flow conditions in the cell are difficult to analyse. But since the flow conditions change the mass transport towards the electrode surface it can be assumed that there is a different whether the gas is flushed directly on the electrode or whether it is not within the direct gas flow of $CO_2$. The sensitivity of the position was analysed by changing the pump speed during electrolysis. The electrode position was not optimised and a reason apart from contaminations might be a too fast gas flow that hinders $CO_2$ to reach the electrode surface. This could also be a reason for the lack of $CH_4$ production on the copper electrode. In order to form $CH_4$, $CO$ needs to remain on the copper step after formation since it is an intermediate for methane production. Another indication in favour for a problem with mass transport is the low current density of the rougher electrodes. During underpotential deposition of $Cu$ the cell conditions were less turbulent compared to $CO_2$ electrolysis because of a lower flow speed of argon and no formation of gas bubbles on the electrode surface. The active area that is accessible for $CO_2$ might be much lower compared to the results of $Cu$ UPD due to hydrogen formation and agglomeration of gas bubbles on the surface that cover the porous layers. There are some minor remarks and limitations about the gas chromatograph. The TC-Detector cannot detect $CO$ with a gas concentration lower than 0.1 % what refers to a peak area of less than 20. For higher concentrations the TCD and FID Back results match better with increasing concentration. For the given limit of 0.1 % $CO$ the deviation between the TCD and the FID Back, which are connected in series, is 15.04 %. The results for 0.1V % are TCD=49.49 % with a peak area of 19.78 and FID Back = 4.45 % with a peak area of 131.98. During some measurements the pressure in the tube system raised from the standard value of 1.07bar to over 1.1bar. The sample stream that the GC injects is constant 1000 $\mu$l but the density and thus the number of molecules dependent on the pressure. The higher the pressure the more molecules are injected. The calibration of the GC is done for a pressure of 1.07 bar, without an increase due to chemical

reactions and thus gaseous reaction products in the cell. This pressure increase is visible in the results, since the total faradaic efficiency exceeds 100 % if the pressure is over 1.1bar. This problem can be avoided by decreasing the reaction time and so the reaction product quantity and thus the pressure raise. A second possibility is to do the calibration for several pressure steps between 1.07 to 1.1bars. In this case more care has to be taken to control the pressure before and after the reduction process. The pressure is supposed to be ambient. Thus, the cell has to be leak tight in order to catch reaction products but no pressure difference to the surroundings should be visible. In literature the pressure is given to be at atmospheric pressure at 1013.25 mbar. The pressure regulator is at some distance in front of the electrochemical cell. It is set to 1.07bars and assumed to be 1013.25 mbar in the cell by accounting for pressure losses in the tube system. Some inconsistencies were observed while measuring the IR-drop of the set-up. The potentiostat software has an automatic tool that measures the IR-drop of the cell with a high frequency scan based on PEIS. While doing manual PEIS scans from lower to higher frequencies the measured valued differ. For copper the differences were about 30 ohms. Due to the low currents for all electrodes throughout this work, this error had a minor influence on the set-up. Secondly, the Nyquist-diagrams shows inductance for all kind of electrodes whose source is unknown. Another problem arises from the concept of the tube system. The tubes systems has to be flushed after experiments for at least 5 minutes to assure that no left over gases from previous experiments are left in dead volumes of the loop. Very high concentrations need longer flushing duration and it is difficult to ensure that all residues as washed out. A GC analysis is therefore suggested in closed loop mode and before the measurements start.

## 4.5 $CO_2$ reduction

$CO_2$ reduction was conducted with a copper sample in order to reproduce literature results and with gold electrodes with several roughness factors to continue Kanan's work on nanoporous gold film electrodes. In this section the results will be classified into the findings of the literature research provided in section 2.4.

### 4.5.1 Summary of results on copper

The results for Copper were used to verify the electrochemical set-up and prove its reliability. The discussion about uncertainties and errors that can be attributed to the set-up was done in the section before. The selectivity for a product depends on several parameters. On copper it is well known that the surface morphology and plane orientation changes the product distribution significantly. Differences between literature results may be allocated to different surface orientation of the electrodes, since this was not analysed and the used copper sample assumed to be polycrystalline. The lack of methane formation is an indication for an absence of absorbed hydrogen molecules at the copper surface. $CH_4$ is formed by adsorbed $CO$ molecules that were just created on the copper surface and in the presence of hydrogen (Hydrogenation). The increasing yield of copper whereas a decline is expected can be interpreted as stripped of $CO$ molecules that do not further react to methane. A reason for the lack of absorbed hydrogen at the copper sites might be found in the flow conditions and the mass transport towards the surface but also in the simultaneous occurring hydrogen evolution reaction. The hydrogen yield is higher and does not seem to disappear with higher voltages what can be allocated to carbon deposition on the copper surface which catalyses hydrogen evolution during electrolysis. Copper catalyses more than the presented products, see 2.2, like $C_2$ compounds. In principle

these products are possible to be measured but the reaction time was most likely too short with 10 to 30 min in order to accumulate enough product gas for analysis in the GC.

### 4.5.2 Summary of results on gold

Figure 4.19 shows the results for all gold electrodes combined with the results of Kanan's group. Regarding Kanan's results for the NPG film, the polycrystalline electrode and RF10 it is possible to see a shift towards a lower overpotential that could be allocated to the roughness factor. On the other hand the results for RF6 showed an even lower overpotential in the

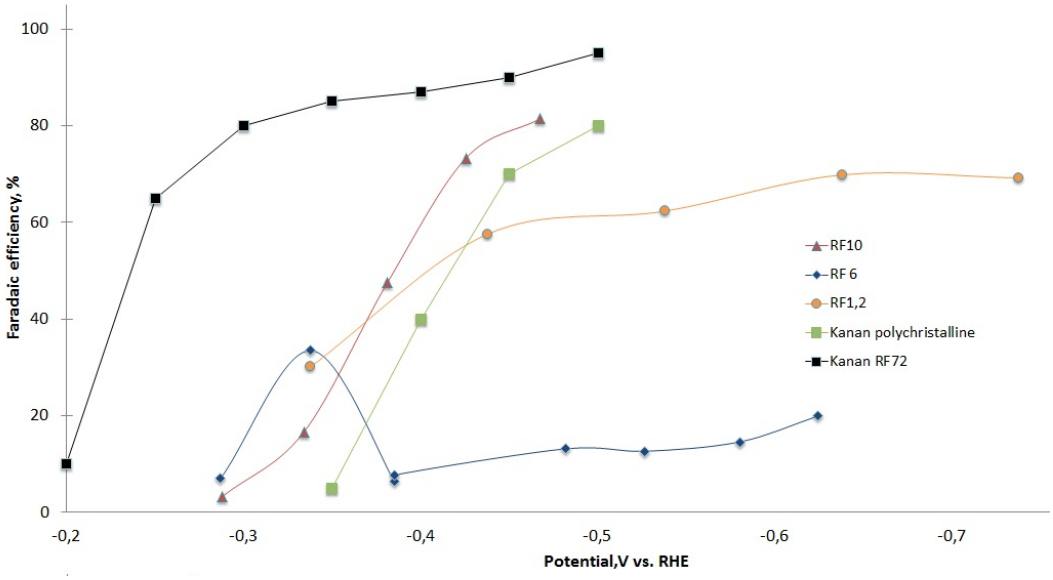


**Figure 4.19:** Summary of results for NPG film electrodes and comparison with literature results

beginning and before deactivation but the electrodes used here and in Kanan's group can hardy be compared. The SEM analysis revealed much bigger nano particles and clusters as product of the electroplating technique. A small decrease of overpotentials is visible what suggests that the catalytic and thermodynamic conditions are changed. The plane evaporated gold electrode has a polycrystalline morphology and low roughness factor. The electrodeposited electrodes are produced from gold oxide and have a nanoporous structure. Regarding the current densities an increase with roughness factor is visible (4.20). Analysing the increase and comparing it with the increase of roughness factor, reveals that the current density is reduced for each electrode. (4.21 The reason for this could be that the nanoporous structure blocks some part of the electrode's surface. Deeper regions of the porous structure are not participating in the reaction. An explanation is the coverage of the surface with gas molecules that accumulate to bubbles and cover and block the active sites and as well cover the entrances to lower areas of the porous structure. The results showed as well deactivation of most of the electrode. The reasons for contaminations are manifold but there are some sources that might be more important in this set-up. The iron conductor is mounted with a copper foil on the electrodes. The glue that is used for the foil was not analysed, neither was the resin that covers the foil. Although the surfaces were cleaned before and after preparation and the resin was not submerged into the electrolyte, it cannot be excluded that the source of contamination is the resin. As a technique to avoid deactivation anodic polarization was introduced in the reduction procedure for RF10 and RF15. Although RF10 showed no deactivation during electrolysis the applied method cannot be considered as a solution, since RF15 showed very low selectivity for CO.

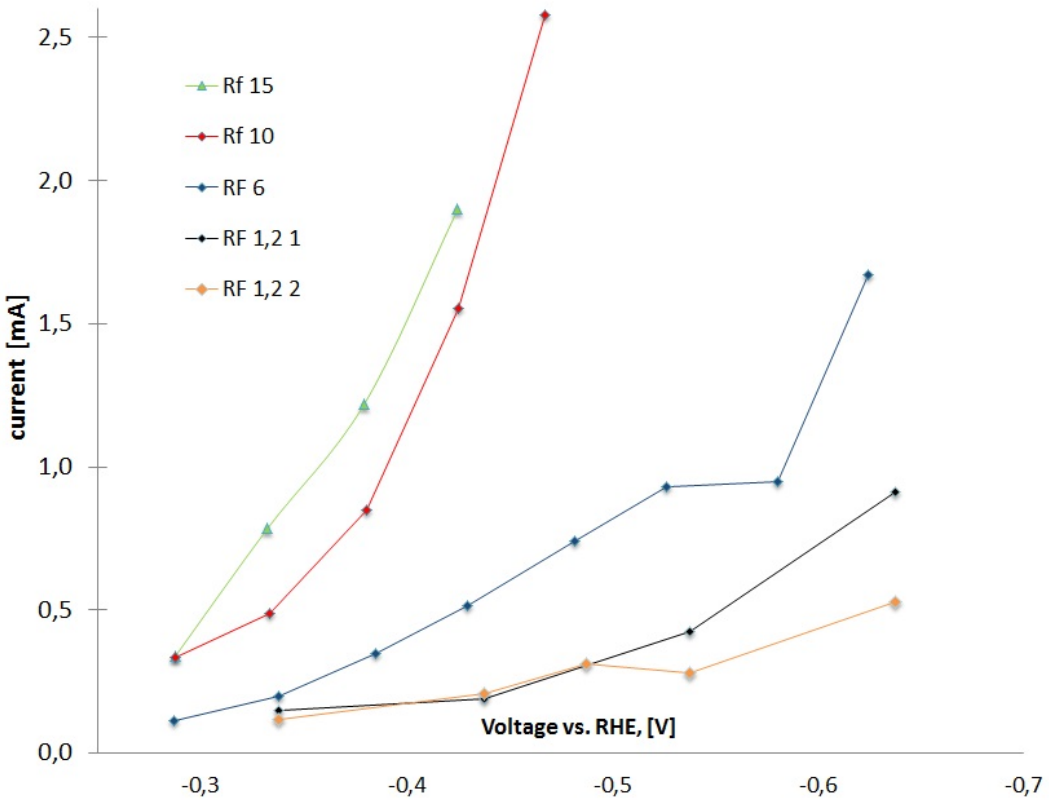


**Figure 4.20:** Comparison of mean currents during electrolysis for different *Au* electrodes plotted against potential vs. RHE.

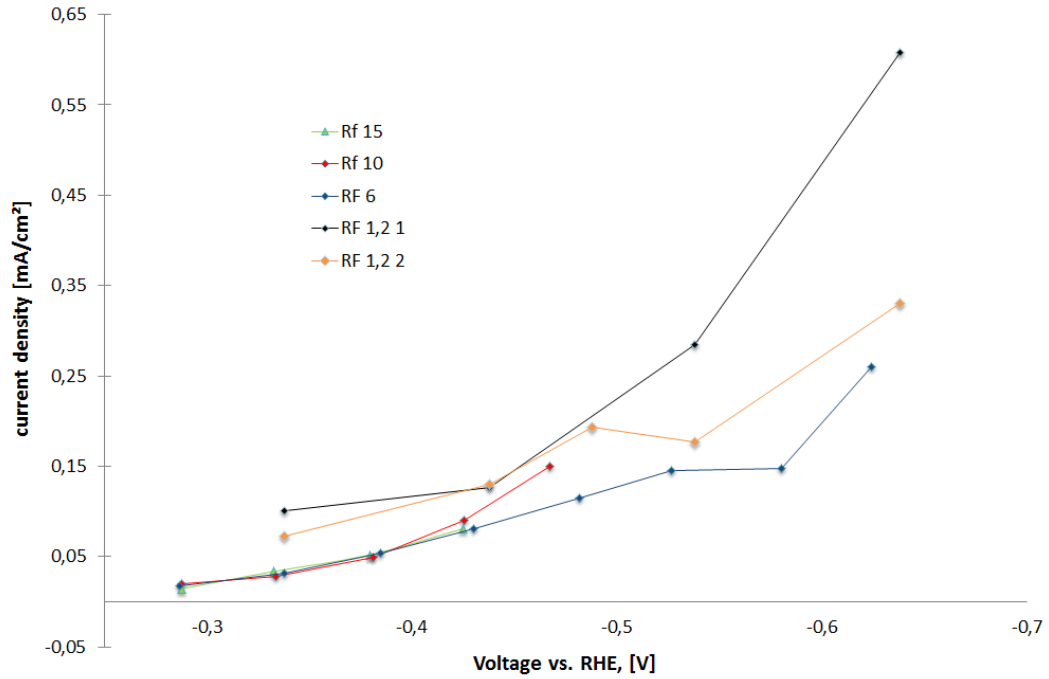


**Figure 4.21:** Comparison of current densities during electrolysis for different *Au* electrodes plotted against potential vs. RHE.

# 5

# Conclusion

## 5.1 Summary

Production of green fuels from $CO_2$ is a promising technique to address a broad range of environmental problems. The question whether this method can be effective regarding these issues depends on the progress within the research of $CO_2$ reduction. Among others, two challenges within the research of electrochemical reduction of $CO_2$ were addressed in this thesis. The first challenge concerns the reduction of high overpotential on various electrode materials and surfaces. The second challenge lies in an increase in current density combined with high selectivity for single products. A promising method in recent research to increase the energy efficiency of the reduction process is the formation of rough, nanoporous films of Au that supposedly reduce the overpotential. Furthermore NPG film electrodes reduce the cost for large scale electrodes since only a few hundred nanometers of Au are needed and the rougher surface increases the current density of the electrode. In the presented thesis work this concept was carried on with the successful production of a porous layer of Au nanoparticle with different roughness factors by electrodeposition of gold ions on a semiconductor substrate. For experiments on these electrodes, a set-up that allows analysis of gaseous products has been verified to work by electrolysis of a copper electrode. A reduction of overpotential directly connected to the roughness cannot be excluded but could also not be proven. The results in this work for different roughness factors of gold electrodes were very similar, but the particle and grain size of Au was the same for all electrodes. This suggests that the dimension of the nano particles might be the dominant factor rather than the roughness factor. The increase of current density due to the increase of surface area seems promising although the raise in current is not proportional to the increase in surface. Problems with mass transport within the porous layer were allocated to this phenomena. The experiments in this work showed the difficulties with the process of electrochemical reduction of $CO_2$. Very little impurities and contaminations can deactivate electrodes and block hydrocarbon production. The susceptibility for deactivation comes from the possibility of a monolayer coverage of foreign atoms that block the active sites of the electrode material and cause, dependent on the type of impurities, a side reaction. For copper, which was used for verification of the set-up, the impurities caused larger hydrogen levels and a change in product distribution. Instead of methane, higher levels of $CO$ were formed, although this could also be traced back to mass transport problems and carbon originated side reactions.

## 5.2 Suggestions for set-up improvements and future prospects for NPG film electrodes

### 5.2.1 Set-up improvements

For the further work with this set-up some modifications can be suggested. A flow meter is necessary in order to have more information about the flow conditions in the cell and the tube system in order to investigate problems with mass transport. Secondly, the cell volume in relation to the electrode size might be a problem for stable and repeatable cell conditions. In that sense it also seems to be important to analyse the placement of the gas bubbler in relation to the shape of the electrodes was identified to be one source of contaminations. Using resin and copper foil that is not made with this purpose in a sensitive electrochemical system should be avoided if possible. An alternative could be to us electrodes out of one piece that do not need any mounting or assembling. In order to reach a higher degree of accuracy for the GC results, either a way to avoid a pressure rise should be found or more calibration points should be taken. A simple way to avoid pressure changes is to use a bigger volume or to decrease the electrode surface submerged into the electrolyte (less products). Problems with contamination were present throughout the experimental work whereas the source could not be identified eventually. Pre-electrolyis in the working electrode compartment in order to remove ion contamination that stays after the applied cleaning method is one possibility to overcome this problem.

### 5.2.2 Future prospects for NPG film electrodes

Au as an electrode material a high catalyst activity and selectivity towards $CO2$ reduction. Gold electrodes of several kinds were shown to be stable over long time measurements and the research direction towards nanostructured catalyst materials seems promising to reduce the overpotential and hence increase the energy efficiency of the reduction process. The determining reason for the reduction of overpotential towards $CO$ formation on gold seems to be the size of the nanoparticles and the structure of the electrode surface, rather than the roughness factor although the results of this work cannot provide a final answer. Thus, as a future research direction could aim on analysing the effects of different particle size and its effect on the enhancement of catalytic activity of Au electrodes. The electrochemical method to produce {NPGfilm electrodes used in this work, creates large nanoparticles and clusters. Other methods were presented and could be used to produce smaller particles and smaller clusters with also higher roughness factors. From an theoretical point of view it is not well understood how the reduction process works. Fundamental understanding will help to develop more efficient catalyst thus theoretical research combined with experimental data in order to understand the connection between the reduction process and the structure of the electrode are necessary. The main goal of this research field is the mitigation of environmental impacts of $CO_2$ by recycling. Practical application though, will require a scale-up of laboratory methods. Due to the requirements of cleanliness and the susceptibility to degradation and deactivation of most catalyst materials, practical application cannot be just adapted by up-scaling. Although the fundamental research has not been successfully done, facts about how this technique could be used in industry processes are important in terms of feasibility. One part of this question is the design of reactors for practical application. There is no final cell or electrode design what makes it difficult to compare results. The cell and electrode designs determine the flow conditions in the cell and thus the $CO_2$ transport towards the electrode. Secondly different

system designs might be a reason for contradictory results on similar electrodes. In summary, nanostructered electrodes seem to be a promising research direction but there a still several challenges to overcome.

# Bibliography


[1] Y. Hori, A. Murata, and R. Takahashi. Formation of hydrocarbons in the electrochemical reduction of carbon-dioxide at a copper electrode in aqueous-solution. *Journal of the Chemical Society-Faraday Transactions I*, 85(8):2309–2326, 1989.

[2] A. A. Peterson, F. Abild-Pedersen, F. Studt, J. Rossmeisl, and J. K. Norskov. How copper catalyzes the electroreduction of carbon dioxide into hydrocarbon fuels. *Energy Environmental Science*, 3(9):1311–1315, 2010.

[3] Y. Chen, C. W. Li, and M. W. Kanan. Aqueous co2 reduction at very low overpotential on oxide-derived au nanoparticles. *Journal of the American Chemical Society*, 134(49):19969–19972, 2012.

[4] Yoshio Hori, Katsuhei Kikuchi, Akira Murata, and Shin Suzuki. Production of methane and ethylene in electrochemical reduction of carbon-dioxide at copper electrode in aqueous hydrogencarbonate solution. *Chemistry Letters*, 15(6):897–898, 1986. C8627 Times Cited:165 Cited References Count:5.

[5] S. Wasmus, E. Cattaneo, and W. Vielstich. Reduction of carbon dioxide to methane and ethene—an on-line ms study with rotating electrodes. *Electrochimica Acta*, 35(4):771–775, 1990.

[6] H. Helmholtz. Ueber einige gesetze der vertheilung elektrischer ströme in körperlichen leitern mit anwendung auf die thierisch-elektrischen versuche. *Annalen der Physik und Chemie*, 165(6):211–233, 1853.

[7] John O'M Bockris and Shahad UM Khan. *Surface Electrochemistry: A Molecular Level Approache*. Springer, 1993.

[8] M. E. Vela, S. L. Marchiano, R. C. Salvarezza, and A. J. Arvia. Growth of columnar gold electrodes by electroreducing hydrous gold oxide layers - kinetics and mechanistic interpretation. *Journal of Electroanalytical Chemistry*, 388(1–2):133–141, 1995.

[9] Falong Jia, Chuanfang Yu, Zhihui Ai, and Lizhi Zhang. Fabrication of nanoporous gold film electrodes with ultrahigh surface area and electrochemical activity. *Chemistry of Materials*, 19(15):3648–3653, 2007.

[10] Carl H. Hamann. Electrochemistry. 1998.

[11] Tomonori Saeki, Kazuhito Hashimoto, Naokazu Kimura, Koji Omata, and Akira Fujishima. Electrochemical reduction of co2 with high current density in a co2 + methanol medium ii. co formation promoted by tetrabutylammonium cation. *Journal of Electroanalytical Chemistry*, 390(1–2):77–82, 1995.

[12] Gamry Instruments. Understanding ir compensation. Technical note, 2012.

[13] Svante Aberg. Measurement of uncompensated resistance and double layer capacitance during the course of a dynamic measurement: correction for ir drop and charging currents in arbitrary voltammetric techniques. *Journal of Electroanalytical Chemistry*, 419(1):99–103, 1996.

[14] D. Britz. ir elimination in electrochemical cells. *Journal of Electroanalytical Chemistry and Interfacial Electrochemistry*, 88(3):309–352.

[15] S. Trasatti and O. A. Petrii. Real surface-area measurements in electrochemistry. *Journal of Electroanalytical Chemistry*, 327(1-2):353–376, 1992.

[16] E. Rouya, S. Cattarin, M. L. Reed, R. G. Kelly, and G. Zangari. Electrochemical characterization of the surface area of nanoporous gold films. *Journal of the Electrochemical Society*, 159(4):K97–K102, 2012.

[17] V. Sudha and M. V. Sangaranarayanan. Underpotential deposition of metals: structural and thermodynamic considerations. *The Journal of Physical Chemistry B*, 106(10):2699–2707, 2002.

[18] J. W. Schultze and D. Dickertmann. Potentiodynamic desorption spectra of metallic monolayers of cu, bi, pb, tl, and sb adsorbed at (111), (100), and (110) planes of gold electrodes. *Surface Science*, 54(2):489–505, 1976.

[19] K. L. N. Phani, S. Mohan, and R. Venkatachalam. Underpotential deposition of copper on electrochemically treated polycrystalline au surfaces. *Proceedings of the Indian Academy of Sciences-Chemical Sciences*, 103(5):677–683, 1991.

[20] S. B. Brummer and A. C. Makrides. Surface oxidation of gold electrodes. *Journal of the Electrochemical Society*, 111(10):1122–1128.

[21] AA Michri, AG Pshenichnikov, and R Kh Burshtein. Determination of the true surface of smooth au electrodes. *Elektrokhimiya*, 8(3):364–366, 1972.

[22] G. Tremiliosi-Filho, L. H. Dall'Antonia, and G. Jerkiewicz. Growth of surface oxides on gold electrodes under well-defined potential, time and temperature conditions. *Journal of Electroanalytical Chemistry*, 578(1):1–8, 2005.

[23] Y. Hori, K. Kikuchi, and S. Suzuki. Production of co and ch4 in electrochemical reduction of co2 at metal-electrodes in aqueous hydrogencarbonate solution. *Chemistry Letters*, (11):1695–1698, 1985.

[24] K. P. Kuhl, E. R. Cave, D. N. Abram, and T. F. Jaramillo. New insights into the electrochemical reduction of carbon dioxide on metallic copper surfaces. *Energy Environmental Science*, 5(5):7050–7059, 2012.

[25] M. Gattrell, N. Gupta, and A. Co. A review of the aqueous electrochemical reduction of co2 to hydrocarbons at copper. *Journal of Electroanalytical Chemistry*, 594(1):1–19, 2006.

[26] W. Tang, A. A. Peterson, A. S. Varela, Z. P. Jovanov, L. Bech, W. J. Durand, S. Dahl, J. K. Norskov, and I. Chorkendorff. The importance of surface morphology in controlling the selectivity of polycrystalline copper for co2 electroreduction. *Phys Chem Chem Phys*, 14(1):76–81, 2012.

[27] Y. Hori, I. Takahashi, O. Koga, and N. Hoshi. Electrochemical reduction of carbon dioxide at various series of copper single crystal electrodes. *Journal of Molecular Catalysis A: Chemical*, 199(1–2):39–47, 2003.

[28] Derek Pletcher. *A first course in electrode processes*. Royal Society of Chemistry, 1991.

[29] N Gupta, M Gattrell, and B MacDougall. Calculation for the cathode surface concentrations in the electrochemical reduction of co2 in khco3 solutions. *Journal of applied electrochemistry*, 36(2):161–172, 2006.

[30] Klaas Jan P. Schouten, Zisheng Qin, Elena Pérez Gallent, and Marc T. M. Koper. Two pathways for the formation of ethylene in co reduction on single-crystal copper electrodes. *Journal of the American Chemical Society*, 134(24):9864–9867, 2012.

[31] David W DeWulf, Tuo Jin, and Allen J Bard. Electrochemical and surface studies of carbon-dioxide reduction to methane and ethylene at copper electrodes in aqueous-solutions. *Journal of The Electrochemical Society*, 136(6):1686–1691, 1989.

[32] Y. Hori, H. Konishi, T. Futamura, A. Murata, O. Koga, H. Sakurai, and K. Oguma. "deactivation of copper electrode" in electrochemical reduction of co2. *Electrochimica Acta*, 50(27):5354–5369, 2005.

[33] G. Kyriacou and A. Anagnostopoulos. Electroreduction of co2 on differently prepared copper electrodes: The influence of electrode treatment on the current efficiences. *Journal of Electroanalytical Chemistry*, 322(1–2):233–246, 1992.

[34] L. M. Chiacchiarelli, Y. Zhai, G. S. Frankel, A. S. Agarwal, and N. Sridhar. Cathodic degradation mechanisms of pure sn electrocatalyst in a nitrogen atmosphere. *Journal of Applied Electrochemistry*, 42(1), 2012.

[35] B. D. Smith, D. E. Irish, P. Kedzierzawski, and J. Augustynski. A surface enhanced roman scattering study of the intermediate and poisoning species formed during the electrochemical reduction of co2 on copper. *Journal of The Electrochemical Society*, 144(12):4288–4296, 1997.

[36] Ryuichi Shiratsuchi, Yoshihisa Aikoh, and Gyoichi Nogami. Pulsed electroreduction of co2 on copper electrodes. *Journal of The Electrochemical Society*, 140(12):3479, 1993.

[37] Y. Garsany, O. A. Baturina, K. E. Swider-Lyons, and S. S. Kocha. Experimental methods for quantifying the activity of platinum electrocatalysts for the oxygen reduction reaction. *Anal Chem*, 82(15):6321–8, 2010.

[38] Yoshio Hori, Akira Murata, Katsuhei Kikuchi, and Shin Suzuki. Electrochemical reduction of carbon dioxides to carbon monoxide at a gold electrode in aqueous potassium hydrogen carbonate. *Journal of the Chemical Society, Chemical Communications*, (10):728–729, 1987.

[39] FJ Uribe, Edward Allen Mason, and Joseph Kestin. Thermal conductivity of nine polyatomic gases at low density. *Journal of physical and chemical reference data*, 19(5):1123–1136, 1990.

[40] E Bich, J Millat, and E Vogel. The viscosity and thermal conductivity of pure monatomic gases from their normal boiling point up to 5000 k in the limit of zero density and at 0.101325 mpa. *Journal of Physical and Chemical Reference Data*, 19(6):1289–1305, 1990.

[41] Y Hori. *Electrochemical CO2 reduction on metal electrodes*, pages 89–189. Springer, 2008.

# Appendices

# .1 Calibration data for gas chromatograph

| | Detector | | | | |
|---|---|---|---|---|---|
| | FID Front | FID Front | FID Front | FID Front | FID Front |
| Compound | $CH_4$ | $C_2H_6$ | $C_2H_4$ | $C_3H_8$ | $C_3H_6$ |
| Concentration | 0. 102 | 0.152 | 0.203 | 0.152 | 0.098 |
| 1. | 1181.75 | 3450.95 | 4712.34 | 5276.46 | 3427.06 |
| 2 | 1206.96 | 3516.32 | 4797.98 | 5366.98 | 3471.92 |
| 3 | 1202.73 | 3505.76 | 4784.32 | 5352.22 | 3467.59 |
| 4 | 1196.63 | 3490.93 | 4765.62 | 5332.18 | 3456.83 |
| 5 | 1196.38 | 3489.93 | 4763.81 | 5330.38 | 3457.81 |
| Standard Deviation | 9.57 | 24.82 | 32.54 | 34.35 | 17.53 |
| Average | 1196.88 | 3490.78 | 4764.81 | 5331.64 | 3456.24 |
| Peak area per mol | 11734.15 | 22965.67 | 23472.01 | 35076.63 | 34953.93 |

**Table 1:** Calibration data for gas chromatograph

| | Detector | | |
|---|---|---|---|
| | FID Back | TCD | TCD |
| Compound | $CH_4$ (CO) | H2 | $CO$ |
| concentration | 0.1 | 0.999 | 0.1 |
| 1 | 2862.95 | 1748.41 | 16.78 |
| 2 | 2893.54 | 1777.57 | 18.89 |
| 3 | 2877.34 | 1772.09 | 18.64 |
| 4 | 2860.39 | 1762.09 | 15.37 |
| 5 | 2852 | 1775.84 | 22.565 |
| Standard Deviation | 16.36 | 12.10 | 2.71 |
| Average | 2869.24 | 1767.20 | 18.45 |
| Peak area per mol | 28129.84 | 1768.97 | 184.52 |

**Table 2:** Calibration data for gas chromatograph